Millimeter-Wave Free-Space Dielectric Characterization

Abstract

Millimeter wave technologies have widespread applications, for which dielectric permittivity is a fundamental parameter. The non-resonant free-space measurement techniques for dielectric permittivity using vector network analysis in the millimeter wave range are reviewed. An introductory look at the applications, significance, and properties of dielectric permittivity in the millimeter wave range is addressed first. The principal aspects of free-space millimeter wave measurement methods are then discussed, by assessing a variety of systems, theoretical models, extraction algorithms and calibration methods. In addition to conventional solid dielectric materials, the measurement of artificial metamaterials, liquid, and gaseous-phased samples are separately investigated. The pros of free-space material extraction methods are then compared with resonance and transmission line methods, and their future perspective is presented in the concluding part.

Key words: Millimeter wave, dielectric, permittivity, free space, quasi-optical, calibration

1. Introduction

The millimeter (mm) wave lies in the range of 30-300 GHz and has conventionally been used in areas of radio astronomy [1-2] and remote sensing [3-4]. With the rapid development of high frequency electronic technologies [5-6], mm-wave technologies have been expanded to new areas of imaging [7-8], radar [9-10], sensor [11], communications [12-14] and detectors [15].

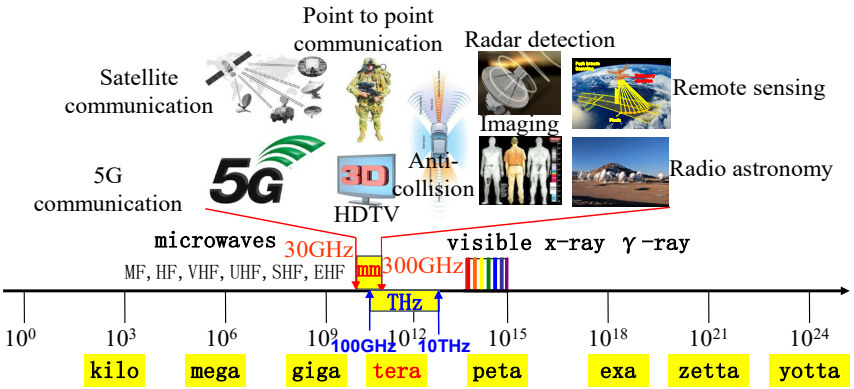

Figure 1: Electromagnetic spectrum and applications of millimeter wave.

A general description of mm-wave applications is presented in Figure 1. A materials' dielectric properties, i.e., complex permittivities, [16]

$$\varepsilon_r = \varepsilon_r' - \mathrm{j}\varepsilon_r'' = \varepsilon_r'\left(1 - j\tan\delta_e\right) \tag{1}$$

are key to achieving new functional applications. The basic mechanisms of permittivity are shown in Figure 2, where the real part of the permittivity ε_r' represents dipole relaxation in the microwave region and lattice vibrations in the terahertz (THz) region. The imaginary part of the permittivity ε_r'', or loss tangent $\tan\delta_e$ relates to the ion

friction effect that contribute to the loss properties of materials. In most cases, permittivities in the low radio frequency band do not change significantly and can be approximated using the static dielectric constant ε_s. In the optical range, permittivities are also stable, and the optical dielectric constant ε_∞ can be used. Albeit, the refractive index n is more frequently used in the optical range [17], and is related to the dielectric constant by $n = \sqrt{\varepsilon_\infty}$. Since the mm-wave band sits in the combined section of relaxation and lattice vibration dynamics, permittivities usually exhibit an observable dispersive property and are of paramount importance to emerging engineering applications. The accurate value of permittivity [18] is critical in designing mm-wave components [19, 20], for example: inaccurate permittivity and loss properties can cause a filter's working frequency to shift, and result in unaccounted insertion loss.

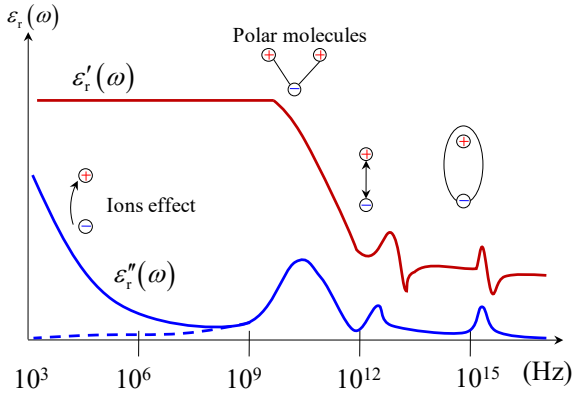

Figure 2: An illustration of frequency dependent dielectric effect.

Dielectric measurement techniques have been discussed in several review articles [21-25], for example: transmission line methods, free-space methods and resonator methods. Both transmission line and resonance-based methods require insertion of sample under test apparatus, such as a waveguide, a broken microstrip line or a closed resonator. Such apparatus is becoming more difficult to manufacture in the mm-wave range, as operational wavelengths continue to decrease. The need for small sample size is also impractical, and the increased loss properties of transmission lines at mm-wave bands can make this method less than attractive. The resonance-based method is really only suitable for small-size and low lossy materials in the mm-wave range, and so the open resonator was developed to enable measurement in this band. However, it actually uses the same theory of Gaussian beam propagation, making it very similar to the free-space method indeed. The reported highest working frequency for the open resonator method is only 300 GHz. The resonance-based method only offers information for discrete frequency points, which makes it dependent on the number of useable modes. By comparison, free-space methods offer broadband characterization capabilities, but may not be a good choice in the microwave range, as large-size samples are required, and the diffraction effect will be more pronounced. However, with regards to measurement practice and electromagnetic physics, the free-space method is more suited to measurement in the mm-wave range - as it is convenient for sample preparation and can achieve wide band material properties.

High frequency semiconductor-based mm-wave electronics take the main role as sources and detectors in mm-wave applications. Therefore, in this review, we focus on

the non-resonant free-space mm-wave dielectric material characterization systems driven mainly by an electronics-based vector network analyzer (VNA). Many aspects of the free-space method have been reviewed and assessed, including the history, development, theory, evolution, extraction methods, and error analysis. We also compared the accuracy and listed some pros and cons of other measurement methods and systems. For most of the cited data, solid and liquid samples dominate, as gaseous sample measurements are made difficult by variations in their concentration impacting permittivity extraction. Metamaterials have demonstrated exciting and attractive electromagnetic properties over the last two decades, and we have briefly touched upon this area in a separate section, as they usually yield unique characteristics that are quite different from homogeneous media.

The remaining parts of this review are organized as follows: Section 2 is a summary of different free-space mm-wave measurement systems; Section 3 is devoted to the methods of complex permittivity extraction; Section 4 discusses the calibration methods of free-space systems; and Section 5 is devoted to measurement results; Section 6 looks at error analysis; Section 7 discusses the properties and measurement methods for metamaterials; Section 8 extends the methods to liquid and gas samples, and Section 9 concludes this review.

2. Free Space Millimeter Wave Systems

The very early free-space system may date back to 1946 [26], with various systems and methods having since been developed [27-72]. A summary of free-space measurement systems is presented in Table I.

2.1 Reflection type

In references [27-29], configured reflection systems were used and their working principles are depicted in Figure 3(a). The transmission and receiving horns were mounted on an arc track, and the sample was placed on a rotational platform. The incident angle is denoted as θ. If the incident electric field is parallel to the incident plane, an angle of incidence can be found for which the reflected field is zero, and this angle is referred as the Brewster angle θ_B. Since the Brewster angle is dependent on the permittivity of sample materials, the permittivity can be retrieved by manipulating mathematics, details of which are presented in Section III.

To use such a method, the following quantities must be measured: (1) the Brewster angle; (2) the effective transmission coefficient at the Brewster angle; (3) the reflection coefficient of the perpendicular and parallel polarizations at the Brewster angle; (4) the wavelength and the thickness of the sample. The method is suitable for low-loss materials. In consideration of multi-reflection effects, a proper correction has to be employed, as shown in Equations (29)-(41) and in Reference [27]. An error analysis was presented in Reference [28] for oblique incidences, but the method requires too many measurements and leads to complicated experimental procedures.

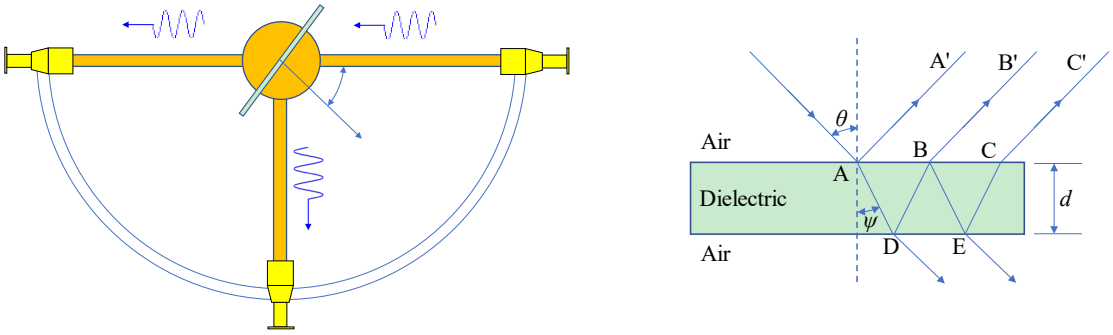

(a) (b)

Figure 3: The diagram of the system in Reference [27]. (a) System layout, (b) multi-reflection model of the signal.

A system very similar to the Brewster-angle-based reflection set-up is discussed in references [33][36][37], which include adaptations first suggested by Cullen [33] and later modifications by [36]. The systems are depicted in Figure 4 (a) and Figure 4 (b). Compared with the Brewster angle method, the procedures are significantly simplified, and are summarized in Section 3. When changing the polarization, phase variation would be observed due to changing horns and waveguide twists. To solve this problem, the reflection part is replaced with a concave reflector. Signals from the Tx-horn will then be reflected back along its own path. In addition, by rotating the sample and the reflector around the beam axis, reflections of different polarization can be measured without changing the length of optical path or the horns and waveguide twists. Although this method is much simpler than the method in [27], it is ill conditioned for finding the product of $\mu_r\varepsilon_r$, where μ_r is the permeability of magnetic materials, which is not within the scope of this review. For this reason, the system in [37] is further improved from [36] enabling measurement of both reflection and transmission, see Figure 4(c). Such modification, makes the signals travel twice along its optical path, and is therefore referred to as double-pass scheme. By using the reflectors, the beams can be effectively refocused so that edge diffractions can be minimized.

A similar system was used in [66], where a metal was used as the reference measurement. Numerical fitting of reflection data was then used to retrieve the permittivity. Such a system was adapted for measurement of high-loss water in the W-band [50], as shown in Figure 5. The permittivity is retrieved by fitting the measurement data to the Cole-Cole model.

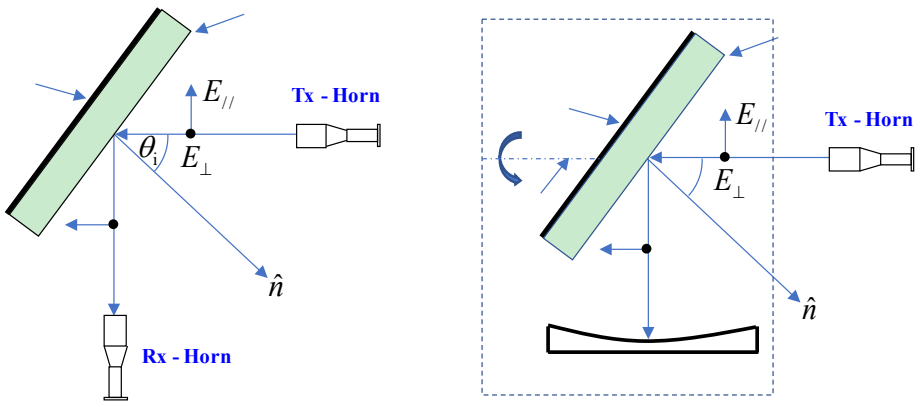

(a) (b)

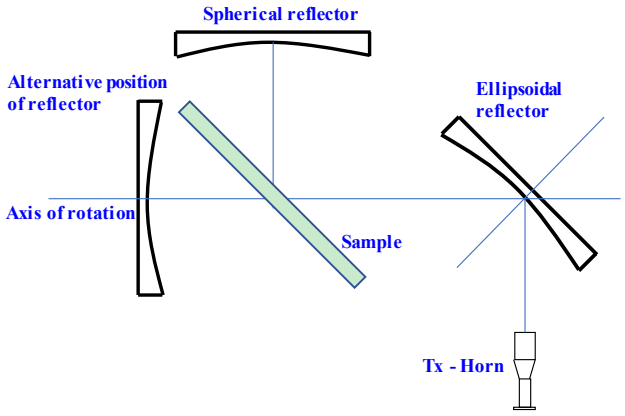

(c)

Figure 4: The evolution of reflection system. (a) Simple metal-backed reflection system. The reflected signal from the sample is received by the Rx-Horn; (b) Concave reflector system. The reflected signal will be refocused by the concave reflector and reflected back to the Tx-Horn; (c) Dual-mode system and it can be used in either reflection mode or transmission mode.

2.2 Transmission type

A combined transmission and reflection configuration was applied to measure and extract permittivities in [35]. However, merely applying a transmission-based set-up is also suitable for permittivity extraction, and a typical system [30] is shown in Figure 6.

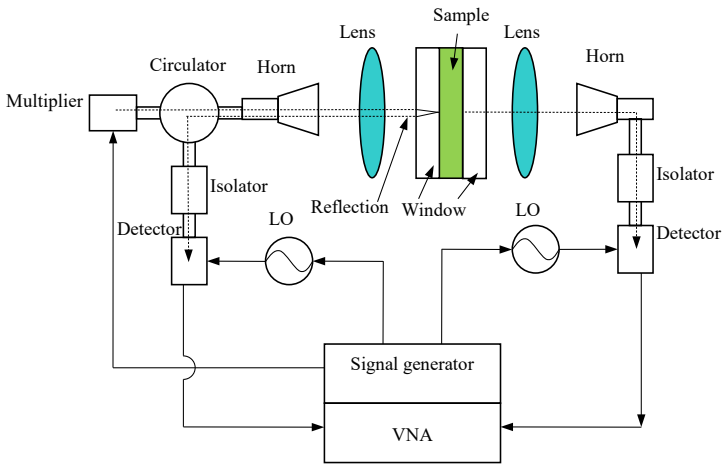

Figure 5: Reflection system for water measurement in the W-band.

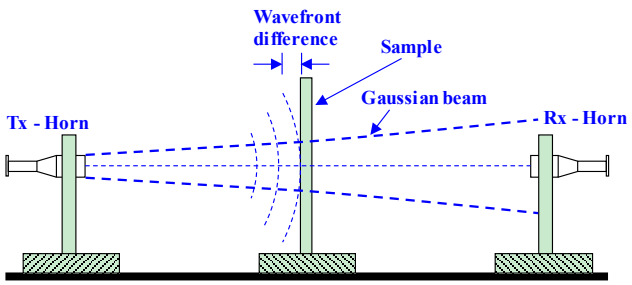

Figure 6: Horn to horn transmission system at normal incidence without focusing elements.

References [31] and [32] proposed a similar system, as shown in Figure 7. The horns are aligned while the sample is tilted to an angle of θ to the boresight direction of the horns. Although the horn antennas radiate spherical waves, the mathematical discussion usually employs planar wave methods (also TEM wave methods). The

Nicolson-Ross-Weir (NRW) procedure [73-74] is a well-used retrieval process based on planar wave theory, which will be discussed in the following section.

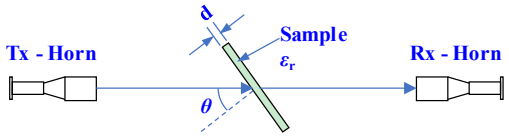

Figure 7: Tilt transmission system without focusing elements.

The systems in Figure 6 and Figure 7 are horn to horn faced transmission systems with no focusing components. Although they can be used to measure the permittivity, drawbacks are also apparent as the spherical wave front of the horn antenna leads to extra phase errors, as depicted in Figure 6. To avoid beam divergence and minimize the transmission loss, beam focusing components were introduced [35], as shown in Figure 8. The focusing lenses are placed at the aperture of the spot-focusing horn antennas and can effectively focus the divergent beam to a very small size. The signal propagation can be modelled using Gaussian beam theory [75], which is usually called a quasi-optical system. In the literature, it happens that only a focusing lens is placed on the transmitting horn side [38], however, it is better to place lenses on both sides.

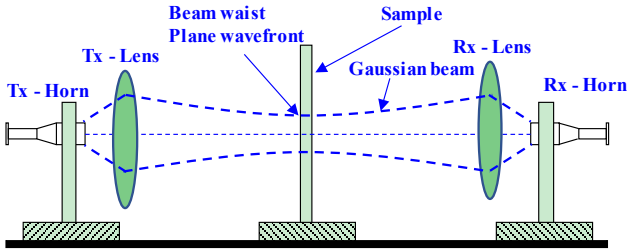

Figure 8: Transmission system with lenses as focusing elements.

The presence of focusing lenses does improve the performance of a free-space system. However, it is found that the lenses also create reflection back to the horns [38]. To further solve this problem, metallic focusing reflectors are used, as illustrated in Figure 9. Such a system is adapted from Figure 4(c). In this setup, the horns are placed on the same side forming a U-shaped system, making it convenient to connect the cables from the horns to a VNA through waveguide connectors. The most important improvement is that the system can eliminate multi-reflection due to the lenses.

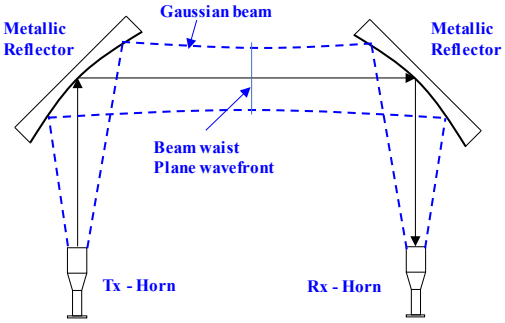

Figure 9: Transmission system with metallic reflectors as focusing elements in the U-shape.

Unfortunately, three problems arise with this system. One is that the beam is slightly distorted at the aperture of the receiving horn; another is that the beam's polarization is not good enough; and the third is that the beam waist between the metallic reflectors is

not small enough. To handle the first issue, the U-shaped configuration can be rearranged to be a Z-shaped one [69]. By using the Z-shaped configuration, the beam quality can be improved. The second problem can be treated by two means, one is using polarizers [51], and the other is to use two more reflectors [47, 53, 63]. As shown in Figure 11, two polarizers are placed before and after the beam travelling through the sample. By using the polarizers, the cross-polarization can be effectively improved, and for high-precision measurements, it is much preferred. However, the cost will be much increased due to the use of polarizers in mm-wave systems.

By using two Z-shaped systems, as shown in Figure 12, the spot size on the sample can be controlled [47, 63]. The design principle is based on Gaussian telescope, as depicted in Chapter 3 of [75]. The Gaussian telescope creates a beam waist the same size of the transmitting horn. Usually, the beam size is several wavelengths large, therefore the required sample size is only a few centimeters.

To further improve the beam quality, a compact test range (CTR) scheme is proposed in [53], where four reflectors are used as well, but with different arrangement [76], as per Figure 13. This configuration provides good polarization isolation and an almost parallel planar wave along the sample, which is even better than the Gaussian beam. By using a serrated edge, the beam quality may be further improved as this can treat edge scattering in a CTR system.

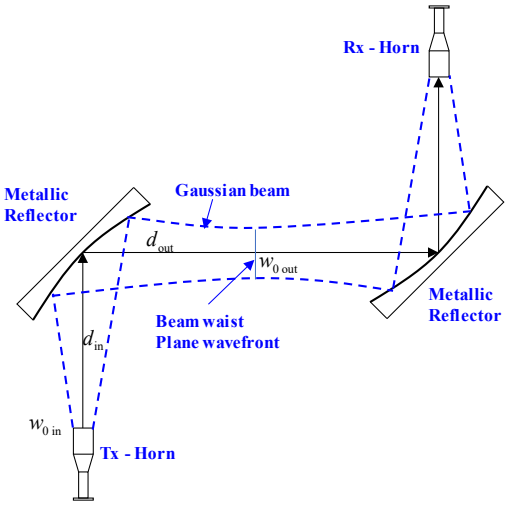

Figure 10: Transmission system with metallic reflectors as focusing elements in the Z-shape.

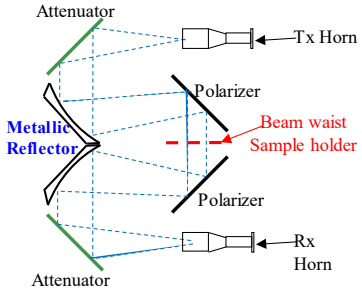

Figure 11: Transmission system with metallic reflectors as focusing elements, using polarizers to enhance polarization purity.

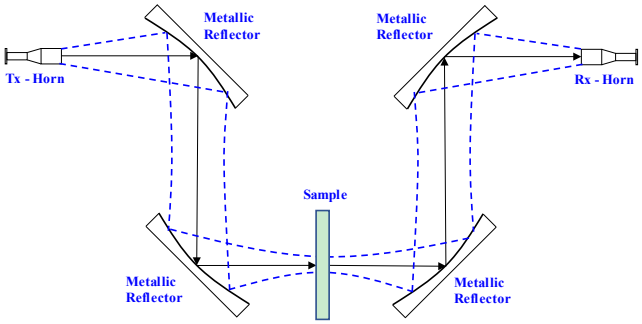

Figure 12: Transmission system with metallic reflectors as focusing elements, using two Z-shaped systems to realize spot beam at the location of the sample.

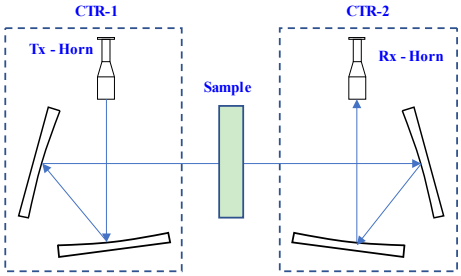

Figure 13: Transmission system with metallic reflectors as focusing elements, using two compact test range to improve the beam quality.

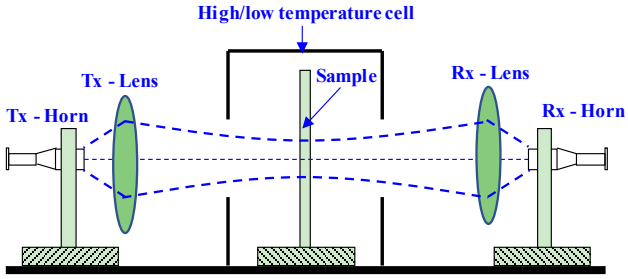

Figure 14: Transmission system with for high/low temperature measurement.

Temperature varied measurement is also possible by using the free space system [42], as shown in Figure 14. The sample is placed inside a high/low temperature cell. The calibration and operation of the system are very similar to the method in [35]. The temperature cell can also be a furnace, as depicted in [72].

The most popular configuration is the spot-focusing transmission system. Using lenses as focusing elements is cost friendly. The transmission model enables full 2-port calibration, leading to measurement of both permittivity and permeability. Systems using metallic reflectors as focusing elements have also received much interest. Their major benefit is the suppression of multireflection, but the cost makes it less popular than the lenses system.

3. Method of extraction

3.1 Extraction methods from reflection measurement

In this review, we restrict ourselves to the permittivity, but occasionally the permeability will be involved in the formulae. This is hardly a problem since one could apply the relative permeability, so that these formulae can be used in a straightforward manner. It was shown that for low-loss and non-magnetic materials (permittivity is

used in our case) the following entities can be observed based on the reflection measurements:

$$\begin{cases} \varepsilon_{\mathrm{r}} = \tan\theta_{\mathrm{B}} \\ \tan\delta = -\dfrac{\lambda_0 \ln r}{\pi d\sqrt{\varepsilon_{\mathrm{r}}+1}} + 0\left(\tan^2\delta\right) \end{cases}, \tag{2}$$

where r is the two-port reflection coefficient electromagnetic wave incident at the Brewster angle, and $0\left(\tan^2\delta\right)$ represents all terms of higher order than $\tan\delta$. For parallel polarized waves, the reflection coefficient is found to be:

$$R_{\parallel} = \frac{\varepsilon_{\mathrm{r}}\cos\theta - \sqrt{\varepsilon_{\mathrm{r}}\mu_{\mathrm{r}} - \sin^2\theta}}{\varepsilon_{\mathrm{r}}\cos\theta + \sqrt{\varepsilon_{\mathrm{r}}\mu_{\mathrm{r}} - \sin^2\theta}}. \tag{3}$$

Allowing the reflection coefficient to be 0, it is found that:

$$\tan^2\theta_{\mathrm{B}} = \frac{\varepsilon_{\mathrm{r}}\left(\varepsilon_{\mathrm{r}} - \mu_{\mathrm{r}}\right)}{\varepsilon_{\mathrm{r}}\mu_{\mathrm{r}} - 1}, \text{when } \varepsilon_{\mathrm{r}} > \mu_{\mathrm{r}}. \tag{4}$$

However, it is not possible to solve for the permittivity unless the permeability is known. In this case, a second formula has to be established. For the perpendicular polarized wave, the reflection coefficient is:

$$R_{\perp} = -\frac{\mu_{\mathrm{r}}\cos\theta - \sqrt{\varepsilon_{\mathrm{r}}\mu_{\mathrm{r}} - \sin^2\theta}}{\mu_{\mathrm{r}}\cos\theta + \sqrt{\varepsilon_{\mathrm{r}}\mu_{\mathrm{r}} - \sin^2\theta}}, \tag{5}$$

at the Brewster angle, it reduces to:

$$\left[R_{\perp}\right]_{\theta=\theta_{\mathrm{B}}} = \frac{\varepsilon_{\mathrm{r}} - \mu_{\mathrm{r}}}{\varepsilon_{\mathrm{r}} + \mu_{\mathrm{r}}}. \tag{6}$$

This coefficient can be measured by placing a metallic plate at the location of the sample. By comparing the reflection from the sample and that from the metallic plate, the value of Equation (6) can readily be obtained.

When $\mu_{\mathrm{r}} > \varepsilon_{\mathrm{r}}$, there is no minimal for Equation (3). The minimal takes place for the perpendicular polarization and can be solved by using Equation (5), and one has:

$$\tan^2\theta_{\mathrm{B}} = \frac{\mu_{\mathrm{r}}\left(\mu_{\mathrm{r}} - \varepsilon_{\mathrm{r}}\right)}{\varepsilon_{\mathrm{r}}\mu_{\mathrm{r}} - 1}, \text{when } \mu_{\mathrm{r}} > \varepsilon_{\mathrm{r}}. \tag{7}$$

and similarly, one has:

$$\left[R_{//}\right]_{\theta=\theta_{\mathrm{B}}} = \frac{\mu_{\mathrm{r}} - \varepsilon_{\mathrm{r}}}{\varepsilon_{\mathrm{r}} + \mu_{\mathrm{r}}}. \tag{8}$$

Measurement of the loss is made in the transmission mode. Taking the first term of transmission, the transmission coefficient can be written as:

$$T_{\parallel} = T_{\mathrm{A}}T_{\mathrm{D}}\mathrm{e}^{\mathrm{j}kd/\cos\psi}, \tag{9}$$

where T_{A} and T_{D} are the transmission coefficients at points A and B respectively, as shown in Figure 3 (b) and $\cos\psi$ can be represented as:

$$\cos\psi = \frac{p}{\sqrt{p^2 + \sin^2\theta}}, \tag{10}$$

where

$$\begin{cases} 2p^2 = \sqrt{\left(a^2 - \sin^2\theta\right)^2 + a^2\tan^2\left(\delta_{\mathrm{e}} + \delta_{\mathrm{m}}\right)} + a^2 - \sin^2\theta \\ a^2 = \varepsilon_{\mathrm{r}}\mu_{\mathrm{r}}\left(1 - \tan\delta_{\mathrm{e}}\tan\delta_{\mathrm{m}}\right) \end{cases}. \tag{11}$$

By taking the logarithm of the absolute of the transmission coefficient, it is found:

$$\ln\left|T_{\parallel}\right| = \ln\left|T_{\mathrm{A}}T_{\mathrm{D}}\right| - \frac{2\pi d}{\lambda}\sqrt{\varepsilon_{\mathrm{r}}\mu_{\mathrm{r}}}\sqrt{\frac{\tan\delta_{\mathrm{e}}+\tan\delta_{\mathrm{m}}}{2\tan\dfrac{\delta_{\mathrm{e}}+\delta_{\mathrm{m}}}{2}}}\frac{\sqrt{p^2+\sin^2\theta}}{2}\tan\frac{\delta_{\mathrm{e}}+\delta_{\mathrm{m}}}{2}, \quad (12)$$

For low loss medium:

$$\sqrt{\frac{\tan\delta_{\mathrm{e}}+\tan\delta_{\mathrm{m}}}{2\tan\left[\left(\delta_{\mathrm{e}}+\delta_{\mathrm{m}}\right)/2\right]}} \approx 1. \quad (13)$$

Setting $\theta = \theta_{\mathrm{B}}$, one has $\left|T_{\mathrm{A}}\right| \approx \left|T_{\mathrm{D}}\right| \approx 1$. This is due to the fact that at the Brewster angle, the reflection is almost zero, and the transmissions are close to unity. By this connection, Equation (12) is reduced to:

$$\ln\left|T_{\parallel}\right| = -\frac{2\pi d}{\lambda}\frac{a^2}{\sqrt{a^2-\sin^2\theta}}\tan\frac{\delta_{\mathrm{e}}+\delta_{\mathrm{m}}}{2}, \quad (14)$$

This approximation provides accuracy of 1% if the total loss is less than 0.1. To separate the losses, the ratio of the parallel reflection to the perpendicular reflection has to be measured:

$$\left[\frac{R_{//}}{R_{\perp}}\right]_{\theta=\theta_{\mathrm{B}}} = \frac{\dfrac{D}{S}\cot^2\theta_{\mathrm{B}} - \dfrac{1}{2}\left(1+\dfrac{1}{\varepsilon_{\mathrm{r}}^2}\right)}{\sqrt{\left[\dfrac{D}{S}\cot^2\theta_{\mathrm{B}} + \dfrac{1}{2}\left(3+\dfrac{1}{\varepsilon_{\mathrm{r}}^2}\right)\right]^2 + \dfrac{4\left(\varepsilon_{\mathrm{r}}\mu_{\mathrm{r}}-1\right)^2}{\varepsilon_{\mathrm{r}}^2 s^2}}}, \quad (15)$$

where

$$\begin{cases} D = \varepsilon_{\mathrm{r}}\tan\delta_{\mathrm{e}} - \mu_{\mathrm{r}}\tan\delta_{\mathrm{m}} \\ S = \mu_{\mathrm{r}}\left(\tan\delta_{\mathrm{e}} + \tan\delta_{\mathrm{m}}\right) \end{cases}. \quad (16)$$

Since the parallel reflection is very small, Equation (15) can be simplified to:

$$D = \frac{S}{2}\left(1+\frac{1}{\varepsilon_{\mathrm{r}}^2}\right)\tan^2\theta_{\mathrm{B}}. \quad (17)$$

Finally, it is found that:

$$\tan\delta_{\mathrm{e}} = \frac{S+D}{\varepsilon_{\mathrm{r}}+\mu_{\mathrm{r}}}. \quad (18)$$

Then, the electric loss can be separated from the magnetic loss by using Equations (14) and (18).

For the system shown in Figure 4, the following formulae can be used:

$$\begin{cases} \dfrac{\mu_{\mathrm{r}}}{\varepsilon_{\mathrm{r}}} = -\dfrac{b}{a}\cot^2\left[kd\sqrt{abQ}\cos\theta_{\mathrm{i}}\right] \\ \mu_{\mathrm{r}}\varepsilon_{\mathrm{r}} = \dfrac{\sin^2\theta_{\mathrm{i}}}{1-ab\cos^2\theta_{\mathrm{i}}} = Q \end{cases}, \quad (19)$$

where,

$$\begin{cases} a = \dfrac{\sqrt{\mu_{\mathrm{r}}\varepsilon_{\mathrm{r}}-\sin^2\theta_{\mathrm{i}}}}{\mathrm{j}\mu_{\mathrm{r}}\cos\theta_{\mathrm{i}}\tan\left[kd\sqrt{\mu_{\mathrm{r}}\varepsilon_{\mathrm{r}}-\sin^2\theta_{\mathrm{i}}}\right]} \\ b = \dfrac{\mathrm{j}\sqrt{\mu_{\mathrm{r}}\varepsilon_{\mathrm{r}}-\sin^2\theta_{\mathrm{i}}}\tan\left[kd\sqrt{\mu_{\mathrm{r}}\varepsilon_{\mathrm{r}}-\sin^2\theta_{\mathrm{i}}}\right]}{\varepsilon_{\mathrm{r}}\cos\theta_{\mathrm{i}}} \end{cases}. \quad (20)$$

It is seen that the retrieve process is much simplified.

For the system in Figure 4(c), it is found that the total reflection and transmission coefficients can be derived as:

$$\begin{cases} R_{\mathrm{T}} = \dfrac{\left(1-P^2\right)R}{1-P^2R^2} \\ T_{\mathrm{T}} = \dfrac{\left(1-R^2\right)P}{1-P^2R^2} \end{cases}, \tag{21}$$

where R stands for reflection coefficient at the interface of either parallel polarization or perpendicular polarization, see Equations (3) and (5), respectively, and P is:

$$P = \exp\left[-\mathrm{j}kd\sqrt{\mu_{\mathrm{r}}\varepsilon_{\mathrm{r}} - \sin^2\theta_{\mathrm{i}}}\right]. \tag{22}$$

The permittivity and permeability can be solved from Equations (21) and (22). Mathematical fitting can also be used for data retrieval.

In a special case of normal incidence, the formalism will be further simplified, but this special case can only measure the permittivity since there is no difference between parallel polarization or perpendicular polarization. For a metal backed case [34], the reflection coefficient reads:

$$R = \frac{\mathrm{j}\tan\left(k\sqrt{\varepsilon_{\mathrm{r}}}d\right) - \sqrt{\varepsilon_{\mathrm{r}}}}{\mathrm{j}\tan\left(k\sqrt{\varepsilon_{\mathrm{r}}}d\right) + \sqrt{\varepsilon_{\mathrm{r}}}}, \tag{23}$$

where ε_{r} is the complex permittivity, k is the wavenumber in free space, and d is the thickness of sample.

3.2 The Nicolson-Ross-Weir method

In the simplest transmission type (Figure 7), the transmission and reflection coefficients are:

$$\begin{cases} T = \dfrac{\left(1-r^2\right)\mathrm{e}^{-\mathrm{j}(\beta_1-\beta_0)d}}{1-r^2\mathrm{e}^{-2\mathrm{j}\beta_1 d}} \\ R = \dfrac{r\left(1-\mathrm{e}^{-2\mathrm{j}\beta_1 d}\right)\mathrm{e}^{-2\mathrm{j}\beta_0 d}}{1-r^2\mathrm{e}^{-2\mathrm{j}\beta_1 d}} \end{cases}, \tag{24}$$

where

$$r = r_{\parallel} = \frac{\beta_1 - \dfrac{\varepsilon_1}{\varepsilon_0}\beta_0}{\beta_1 + \dfrac{\varepsilon_1}{\varepsilon_0}\beta_0}, \tag{25}$$

for parallel polarization, and for perpendicular polarization:

$$r = r_{\perp} = \frac{\beta_0 - \beta_1}{\beta_0 + \beta_1}. \tag{26}$$

One then has:

$$\begin{cases} \beta_1 = \dfrac{2\pi}{\lambda_0}\sqrt{\dfrac{\varepsilon_1}{\varepsilon_0} - \sin^2\theta} \\ \beta_0 = \dfrac{2\pi}{\lambda_0}\cos\theta \end{cases}, \tag{27}$$

where

$$\varepsilon_1 = \varepsilon_0\varepsilon_{\mathrm{r}}\left(1 - j\tan\delta\right). \tag{28}$$

Therefore, the link between the permittivity and the transmission coefficient has been established.

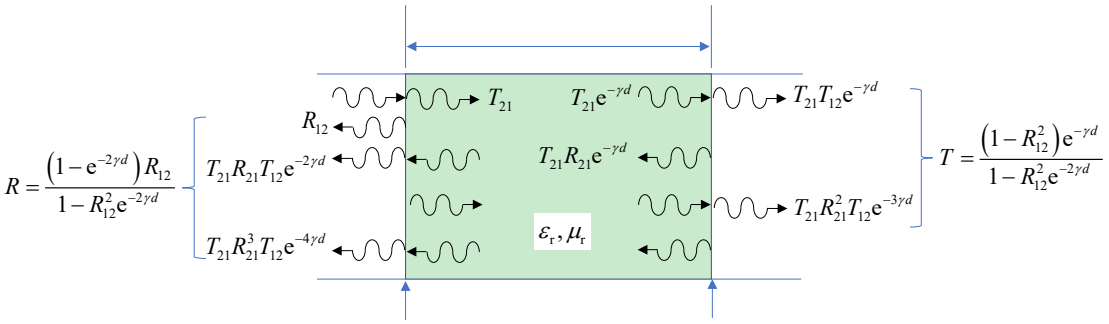

Figure 15: A general description of the multi-reflection model.

For most refocusing systems, the planar wave model can be used to analyze the multi-reflection inside the sample, as shown in Figure 15. The resultant reflection and transmission coefficients can be written as:

$$\begin{cases} R=\dfrac{(1-e^{-2\gamma d})R_{12}}{1-R_{12}^2e^{-2\gamma d}} \\ T=\dfrac{(1-R_{12}^2)e^{-\gamma d}}{1-R_{12}^2e^{-2\gamma d}} \end{cases}, \tag{29}$$

where the reflection of a plane wave on interface 1 is:

$$R_{12}=\frac{\sqrt{\mu_r}-\sqrt{\varepsilon_r}}{\sqrt{\mu_r}+\sqrt{\varepsilon_r}}, \tag{30}$$

and the wave propagation coefficient is:

$$\gamma=\mathrm{j}2\pi\sqrt{\varepsilon_r\mu_r}/\lambda\,. \tag{31}$$

Given that the system is calibrated, the measured reflection and transmission coefficients by a vector network analyzer (VNA) are expressed as S_{11} and S_{21} respectively. Analytical methods can be used to extract the permittivity and permeability. The NRW method was proposed by Nicolson, Ross and Weir [73-74]. Let X to be:

$$X=\frac{1-(S_{21}+S_{11})(S_{21}-S_{11})}{(S_{21}+S_{11})-(S_{21}-S_{11})}=\frac{1+S_{11}^2-S_{21}^2}{2S_{11}}. \tag{32}$$

denote

$$\begin{cases} \Gamma=X\pm\sqrt{X^2-1} \\ z=\dfrac{(S_{21}+S_{11})\text{-}\Gamma}{1\text{-}(S_{21}+S_{11})\Gamma} \end{cases}. \tag{33}$$

It is found that:

$$\begin{cases} \dfrac{\mu_r}{\varepsilon_r}=\left(\dfrac{1+\Gamma}{1-\Gamma}\right)^2=C_1 \\ \varepsilon_r\mu_r=\left[\dfrac{\mathrm{j}c}{\omega d}\ln\left(\dfrac{1}{z}\right)\right]^2=C_2 \end{cases}. \tag{34}$$

Therefore, one has:

$$\begin{cases} \mu_{\mathrm{r}} = \sqrt{C_1 C_2} = \dfrac{\mathrm{jc}}{\omega d}\ln\left(\dfrac{1}{z}\right)\left(\dfrac{1+\Gamma}{1-\Gamma}\right) \\ \varepsilon_{\mathrm{r}} = \sqrt{\dfrac{C_2}{C_1}} = \dfrac{\mathrm{jc}}{\omega d}\ln\left(\dfrac{1}{z}\right)\left(\dfrac{1-\Gamma}{1+\Gamma}\right) \end{cases}. \tag{35}$$

To select the right Γ, one needs to make sure $|\Gamma| \le 1$. In addition, the phase is undefined since we have:

$$\ln\left(\frac{1}{z}\right) = \ln\left|\frac{1}{z}\right| + \mathrm{j}(\theta + 2n\pi), n = 0, \pm 1, \pm 2, \cdots. \tag{36}$$

To determine the right *n*, one could resort to the group delay defined by:

$$\tau_{\mathrm{Cal}} = \frac{\mathrm{d}k}{\mathrm{d}\omega} = d\frac{\mathrm{d}}{\mathrm{d}f}\left(\frac{f}{\mathrm{c}}\sqrt{\varepsilon_{\mathrm{r}}\mu_{\mathrm{r}}}\right) = \frac{d}{c}\left(\sqrt{\varepsilon_{\mathrm{r}}\mu_{\mathrm{r}}} + f\frac{\mathrm{d}\sqrt{\varepsilon_{\mathrm{r}}\mu_{\mathrm{r}}}}{\mathrm{d}f}\right). \tag{37}$$

for free-space transmission, and the measured group delay is:

$$\tau_{\mathrm{Meas}} = -\frac{1}{2\pi}\frac{\mathrm{d}\varphi_{\mathrm{Meas}}}{\mathrm{d}f}. \tag{38}$$

The value of *n* can be determined by comparing the calculated and measured group delay.

3.3 Improved techniques

It was reported that abnormal values were found in measurement [77] using the NRW method. The frequency distance between two adjacent abnormal values is close to:

$$\Delta f = f_{n+1} - f_n = \frac{(n+1)\mathrm{c}}{2\sqrt{\varepsilon_{\mathrm{r}}\mu_{\mathrm{r}}}d} - \frac{n\mathrm{c}}{2\sqrt{\varepsilon_{\mathrm{r}}\mu_{\mathrm{r}}}d} = \frac{\mathrm{c}}{2\sqrt{\varepsilon_r\mu_r}d}. \tag{39}$$

It was found that the spikes at these frequencies originate from the factor of C_1, see Figure 1 and Figure 2 in [77]. This is particularly serious for low-loss or thin samples. To resolve this problem, an improved method was proposed:

$$\begin{cases} \dfrac{\mu_{\mathrm{r\_eff}}}{\varepsilon_{\mathrm{r\_eff}}} = \left(\dfrac{1+\Gamma}{1-\Gamma}\right)^2 = C_1 \\ \varepsilon_{\mathrm{r\_eff}}\mu_{\mathrm{r\_eff}} = \left[\dfrac{\mathrm{jc}}{\omega d}\ln\left(\dfrac{1}{z}\right)\right]^2 = C_2 \end{cases}. \tag{40}$$

Therefore, one has:

$$\begin{cases} \mu_{\mathrm{r}} = \mu_{\mathrm{r\_eff}} = 1 \\ \varepsilon_{\mathrm{r}} = \varepsilon_{\mathrm{r\_eff}}\mu_{\mathrm{r\_eff}} = \left[\dfrac{\mathrm{jc}}{\omega d}\ln\left(\dfrac{1}{z}\right)\right]^2 \end{cases}. \tag{41}$$

For materials $\mu_{\mathrm{r}} = 1$, a more general expression is:

$$\begin{cases} \mu_{\mathrm{r}} = \mu_{\mathrm{r\_eff}} = 1 \\ \varepsilon_{\mathrm{r}} = \varepsilon_{\mathrm{r\_eff}}\left(\mu_{\mathrm{r\_eff}}\right)^n = \left(\dfrac{1-\Gamma}{1+\Gamma}\right)^{1-n}\left[\dfrac{\mathrm{jc}}{\omega d}\ln\left(\dfrac{1}{z}\right)\right]^{n+1} \end{cases}. \tag{42}$$

When *n*=1, the permittivity is corresponding to Equation (41); when *n*=0, the permittivity is corresponding to Equation (35); and for *n*=-1, the permittivity is corresponding to the case in [78]. It was observed that when *n* approached 1, the inaccuracy peaks' amplitudes decreased [77]. Actually, a very similar explicit form has been derived, also assuming $\mu_{\mathrm{r}} = 1$, see Equation (24) in [79]. The expression falls in the case of *n*=1.

Unfortunately, this method assumes $\mu_r = 1$, which implies that only non-magnetic materials can be measured. Therefore, it does not serve as a general method.

3.4 Numerical methods

It is preferred to have closed-form formulae for retrieve. However, the instability of NRW is obvious. The improved method only works for cases when $\mu_r = 1$. With the remarkable progress in computational capability, numerical methods are also time efficient. It could be either least square error technique or solving non-linear equations.

In [80], a stable iterative method was proposed for non-magnetic materials. The ideal equation between measured S-parameter and theoretical model can be written as:

$$\frac{1}{2}\left[\left(S_{21}+S_{12}\right)+\beta\left(S_{11}+S_{22}\right)\right]=\frac{\mathrm{e}^{-\gamma d}\left(1-R_{12}^{2}\right)+\beta\left(1-\mathrm{e}^{-2\gamma d}\right)}{1-R_{12}^{2}\mathrm{e}^{-2\gamma d}}, \tag{43}$$

where β is the ratio factor. The error function can therefore be defined as:

$$F\left(\varepsilon_r',\varepsilon_r'\right)=\frac{1}{2}\left[\left(S_{21}+S_{12}\right)+\beta\left(S_{11}+S_{22}\right)\right]-\frac{\mathrm{e}^{-\gamma d}\left(1-R_{12}^{2}\right)+\beta\left(1-\mathrm{e}^{-2\gamma d}\right)}{1-R_{12}^{2}\mathrm{e}^{-2\gamma d}}. \tag{44}$$

Writing the error function to:

$$F\left(\varepsilon_r',\varepsilon_r''\right)=f\left(\varepsilon_r',\varepsilon_r''\right)+\mathrm{j}g\left(\varepsilon_r',\varepsilon_r''\right). \tag{45}$$

The corresponding Jacobian matrix is:

$$\mathbf{J}=\begin{vmatrix}\dfrac{\partial f\left(\varepsilon_r',\varepsilon_r''\right)}{\partial\varepsilon_r'} & \dfrac{\partial f\left(\varepsilon_r',\varepsilon_r''\right)}{\partial\varepsilon''}\\ \dfrac{\partial g\left(\varepsilon_r',\varepsilon_r''\right)}{\partial\varepsilon_r'} & \dfrac{\partial g\left(\varepsilon_r',\varepsilon_r''\right)}{\partial\varepsilon''}\end{vmatrix}. \tag{46}$$

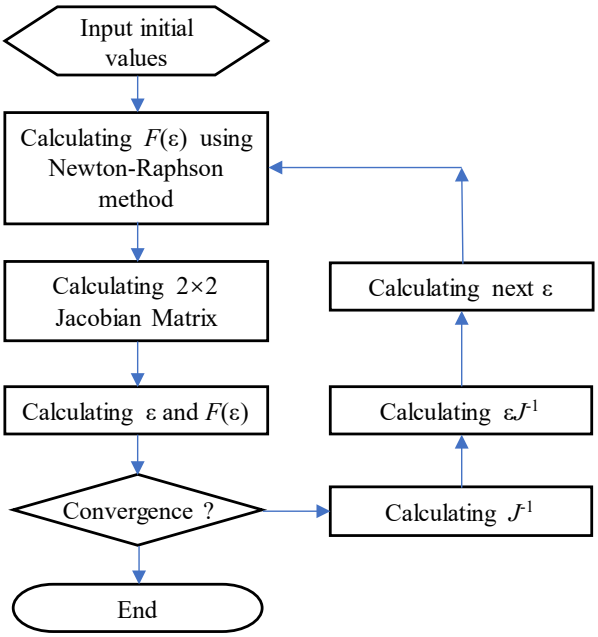

Figure 16: The flowchart for iteration.

The flowchart of the iteration is shown in Figure 16. The method can be extended to retrieve both permittivity and permeability. After calibration, the four elements of the S-parameter matrix will be measured. More than four equations could be defined, being sufficient to solve for fours variables. Other forms of error functions may also be used, and we apologize to those authors whose work is not included in this review.

The least square error method is to compare the measured S-parameters with the fitted ones. The objective functions may take the form of:

$$\chi^2 = \frac{1}{n}\sum_{i=1}^{n}\left[\begin{array}{l}\left(\left|S_{11iM}\right|-\left|S_{11iE}\right|\right)^2+\left(\left|\varphi_{11iM}\right|-\left|\varphi_{11iE}\right|\right)^2 \\ +\left(\left|S_{21iM}\right|-\left|S_{21iE}\right|\right)^2+\left(\left|\varphi_{21iM}\right|-\left|\varphi_{21iE}\right|\right)^2\end{array}\right], \tag{47}$$

where n is the number of spectral points, the subscripts M and E stand for measurement and estimation, respectively [63]. Minimization of the objective function may be done by least square fitting using a Levenberg-Marquardt algorithm [81].

3.5 Retrieval method for multi-layer structure

For liquid samples [54,71] or very thin samples [35], a multi-layer structure has to be used. For instance, liquid must be enclosed using window materials, forming a window-liquid-window structure. Such a structure can be modelled as per Figure 17.

A very common technique is the ABCD matrix analysis method (or transfer matrix). This method was proposed in [35] and has since been used in many publications [51, 52, 54, 69]. Another method proposed by Liu et al [71] is using the signal-flowchart technical, which is equivalent to the ABCD matrix.

The ABCD matrix of the assembly $\mathbf{T}_a$ is:

$$\mathbf{T}_a = \mathbf{T}_1 \cdot \mathbf{T}_2 \cdot \mathbf{T}_3. \tag{48}$$

It is related to the S-parameters of the assembly by:

$$\mathbf{T}_a = \begin{bmatrix} A_a & B_a \\ C_a & D_a \end{bmatrix} = \frac{1}{2S_{21a}}\begin{bmatrix} \left(1+S_{11a}\right)\left(1-S_{22a}\right)+S_{11a}S_{22a} & Z_0\left[\left(1+S_{11a}\right)\left(1+S_{22a}\right)-S_{11a}S_{22a}\right] \\ \dfrac{\left(1-S_{11a}\right)\left(1-S_{22a}\right)-S_{11a}S_{22a}}{Z_0} & \left(1-S_{11a}\right)\left(1+S_{22a}\right)+S_{11a}S_{22a} \end{bmatrix}. \tag{49}$$

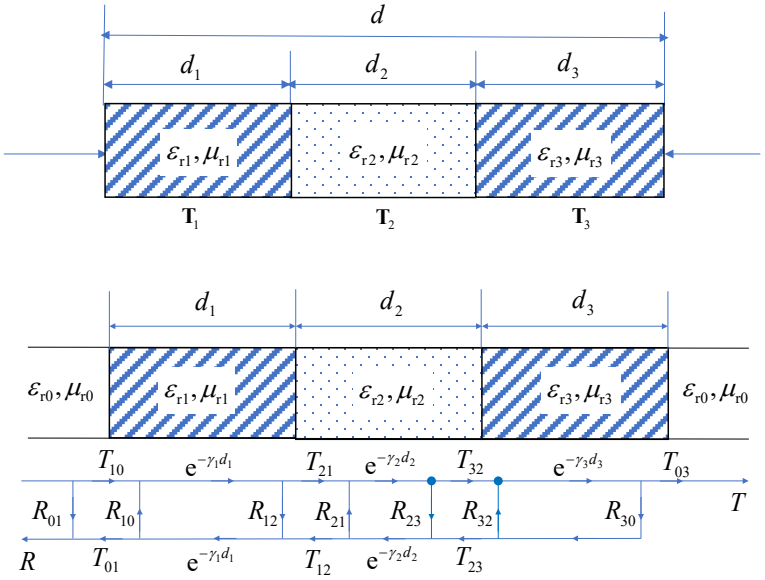

Figure 17. Methods modeling multi-layer structure. (a) ABCD matrix method; (b) signal flow chart method.

For any slab of sample, the ABCD matrix is:

$$\mathbf{T} = \begin{bmatrix} A & B \\ C & D \end{bmatrix} = \begin{bmatrix} \dfrac{e^{\gamma L}+e^{-\gamma L}}{2} & Z\dfrac{e^{\gamma L}-e^{-\gamma L}}{2} \\ \dfrac{e^{\gamma L}-e^{-\gamma L}}{2Z} & \dfrac{e^{\gamma L}+e^{-\gamma L}}{2} \end{bmatrix}, \tag{50}$$

where

$$\begin{cases} \gamma = \mathrm{j}\dfrac{\omega}{\mathrm{c}}\sqrt{\varepsilon_{\mathrm{r}}\mu_{\mathrm{r}}} \\ Z = \sqrt{\mu_{\mathrm{r}}/\varepsilon_{\mathrm{r}}} \end{cases}. \tag{51}$$

By using Equation (48), one has:

$$\mathbf{T}_2 = \mathbf{T}_1^{-1} \cdot \mathbf{T}_{\mathrm{a}} \cdot \mathbf{T}_3^{-1}. \tag{52}$$

It can be converted to the S-parameter of the sample by:

$$\mathbf{S}_{\mathrm{s}} = \begin{bmatrix} S_{11\mathrm{s}} & S_{21\mathrm{s}} \\ S_{12\mathrm{s}} & S_{22\mathrm{s}} \end{bmatrix} = \begin{bmatrix} \dfrac{A+B/Z_0-CZ_0-D}{A+B/Z_0+CZ_0+D} & \dfrac{2(AD-BC)}{A+B/Z_0+CZ_0+D} \\ \dfrac{2}{A+B/Z_0+CZ_0+D} & \dfrac{-A+B/Z_0-CZ_0+D}{A+B/Z_0+CZ_0+D} \end{bmatrix}. \tag{53}$$

The following steps can be used to retrieve the permittivity and permeability:

Step-1: Calibrate and do the measurement to obtain the S-parameter of the assembly $\mathbf{S}_{\mathrm{a}}$;

Step-2: Calculate $\mathbf{T}_{\mathrm{a}}$ using Equation (48), and calculate the ABCD matrix $\mathbf{T}_1$ and $\mathbf{T}_2$ using Equation (50);

Step-3: Calculate the ABCD matrix of the sample $\mathbf{T}_{\mathrm{s}}$ by using Equation (52);

Step-4: Calculate the S-parameter of the sample $\mathbf{S}_{\mathrm{s}}$ by using Equation (53);

Step-5: Calculate the permittivity and permeability using either theoretical model or numerical methods.

4. Calibration Methods

Any accurate measurement is based on good calibration. Many calibration methods have been discussed in the literature [82-90]. In principle, the two-port calibration methods for coaxial line connected systems, may also be used in transmission mode free-space systems. The purpose of calibration is to make sure the measurement is specific to the surface of the material under test, as shown in Figure 18. It is also intended to remove measurement errors as much as possible. The majority of measurements used the through-reflection-line (TRL) method. The through-reflection-matching (TRM) method was also frequently applied. These methods are based on the 8-term error model, which has been clearly described in [91]. Occasionally, the line-reflection-line (LRL) method was also used [46,52], and self-calibration techniques such as LNN were also proposed [86].

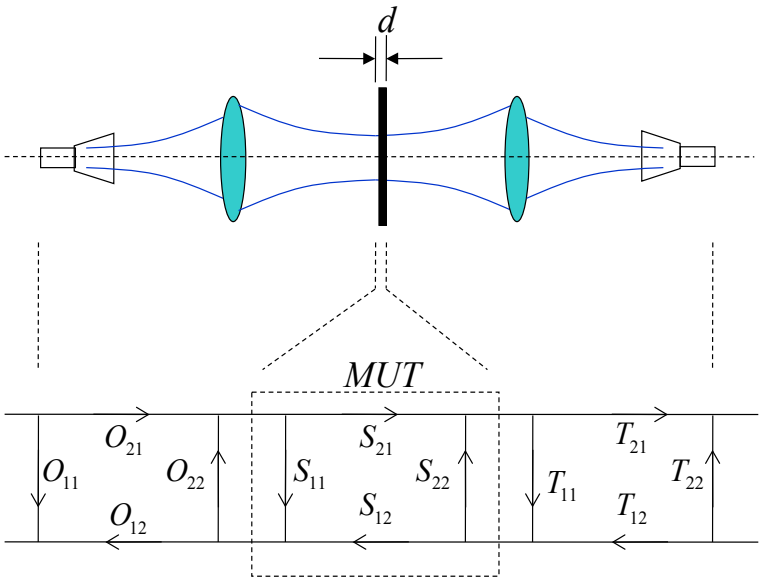

Figure 18: A calibration model for free-space measurement.

The TRL method is illustrated in Figure 19(a), where the last step requires a displacement of one feed horn from its best position. This method has two drawbacks, one is that the precision required for mechanical movement of the horn is markedly high, the other, is that the displacement of the horn actually alters the optical length of the beam radiated from the horn, which would slightly affect the beam quality. To handle this problem the TRM method may be used, as shown in Figure 19(b), where a matching load is used to replace the line step. This option does however require very high-quality absorbers. In [87], a so-called self-calibration technique referred to as the LNN method was discussed, as shown in Figure 19(c). The calibration requires through and several reflectors placed at 3 different locations. Such a method does not change the optical length of the beam.

As a complementary addition to the aforesaid methods, time-domain gating can be employed to filter residual reflections [88]. This approach applies time-domain gating alongside measurements of a metal plate and an empty fixture, to determine the error adapters of the free-space fixture. By filtering off the residual reflections at the throat of the horn and other connectors, the ripples can be much improved. Consequently, the measurement accuracy of the permittivity can be improved accordingly.

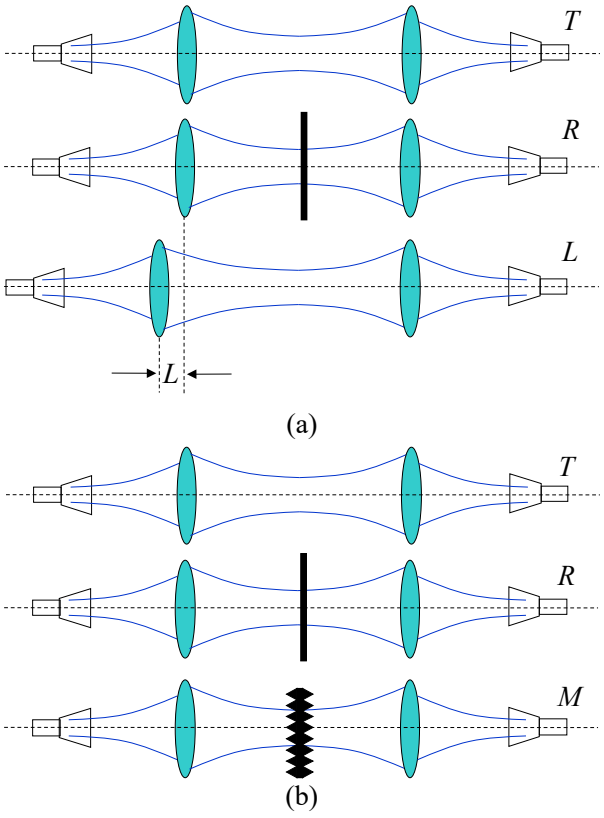

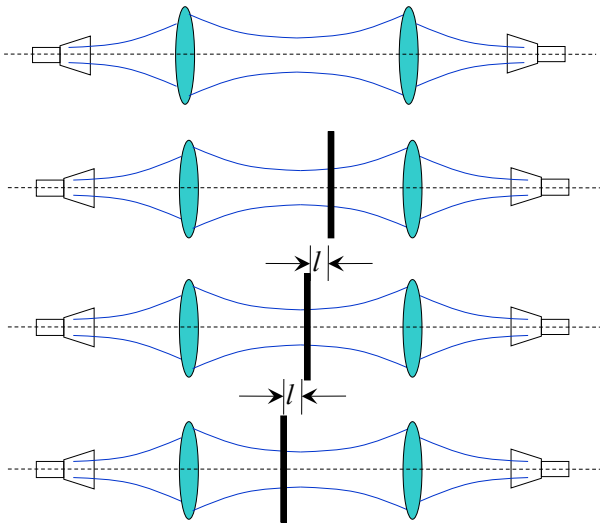

(c)

Figure 19: Setup of the calibration methods. (a) TRL; (b) TRM; (c) LNN.

In actuality, a very simple method can also be used for calibration, i.e., baseline measurement, either on open path or metal reflection. This type of calibration has been used widely [47, 49-51, 54, 64, 69-71]. If the VNA is already calibrated using the SLOT method, the free-space system would provide better accuracy. Further improvement may also be achieved by using time-domain gating technique. Comparing the transmission coefficients of the sample S_{21_s} to that of the baseline S_{21_a}, the real coefficient can be obtained:

$$S_{21} = \frac{S_{21\_s}}{S_{21\_a}} \mathrm{e}^{\mathrm{j}k_0 d} . \tag{54}$$

Since the reference planes for measuring the sample and measuring the open air are different by a distance of d (the thickness of the sample), a phase delay $\mathrm{e}^{\mathrm{j}k_0 d}$ has to be added. For the reflection coefficients, there is no need to consider the phase delay since the reference planes are the same for both measurements. Therefore, both S_{21} and S_{11} can be measured.

Actually, for non-magnetic materials, one only needs to measure either the reflection or transmission coefficient. By using numerical methods for extraction, the permittivity can then be retrieved.

In reference [62], a time-domain measurement technique was proposed for use, even without any scheme of calibration. The underlying principle is to track various reflection and transmission power peaks, where with the aid of closed form relations and an automatic optimization algorithm, the complex permittivity can be obtained. An illustration of the time-domain signal of reflection and transmission is shown in Figure 20. As seen from Figure 15, the first and second reflection peaks are R_{12} and $T_{21}R_{21}T_{12}\mathrm{e}^{-2\gamma d}$. Similarly, the first and second transmission peaks are $T_{21}T_{12}\mathrm{e}^{-\gamma d}$ and $T_{21}R_{21}^2T_{12}\mathrm{e}^{-3\gamma d}$. Therefore, one has:

$$\begin{cases} k = \sqrt{\dfrac{P_{\mathrm{r1}}P_{\mathrm{t2}}}{P_{\mathrm{t1}}P_{\mathrm{r2}}}} = \dfrac{\left|T_{21}R_{21}^2T_{12}\mathrm{e}^{-3\gamma d}\right| \cdot \left|R_{12}\right|}{\left|T_{21}R_{21}T_{12}\mathrm{e}^{-2\gamma d}\right| \cdot \left|T_{21}T_{12}\mathrm{e}^{-\gamma d}\right|} = \dfrac{\left|R_{12}R_{21}\right|}{\left|T_{21}T_{12}\right|} \\ \Delta t \approx \dfrac{2d}{\mathrm{c}\sqrt{\varepsilon_{\mathrm{r}}'}} \end{cases} . \tag{55}$$

Time domain methods are also discussed in reference [92], which can be applied in the millimeter wave measurements.

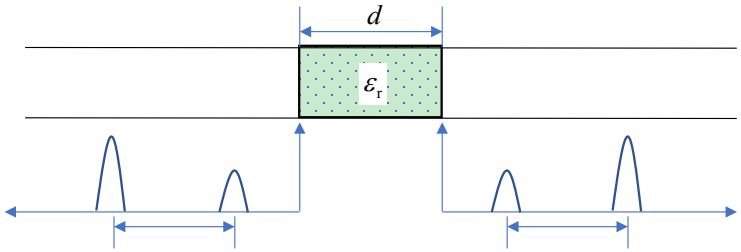

Figure 20: A time-domain illustration of multi-reflection and multi-transmission.

The thickness and permittivity can be derived from Equation (55). To use this method, the thickness of the sample must be considered as this affects the time resolution. The minimum required thickness derived in [62] is $d_{\min} = 10.71/\sqrt{\varepsilon_r'}$. In practice, this needs a very thick sample, although that is not a key drawback. In addition, this method can be extended to calibrate the system, and the accuracy can be further improved. Even for a calibrated system, the multi-reflection or multi-transmission phenomenon may still be observed in the time domain.

5. Results and Discussion

In Table II, much of the published data from the literature is summarized. The measurements covered a broadband frequency range, and a variety of versatile materials commonly used in microwave systems.

There are many interesting points observed. For the real part, most systems provide good accuracy, the majority of which are within 5.0% uncertainty, with some providing even higher accuracy. This is good evidence that the free-space system is suitable for dielectric measurement in the mm-wave range. Many references give very similar measurement results. Taking Teflon as an example, the value at 94 GHz is 2.07 in Ref. [30], and 2.065 in Ref. [31]. Such corroboration suggests a good repeatability of free space methods. In contrast, it is noticeable that loss tangent does not maintain very good uncertainty levels, with many results showing more than 20%. Many published measurements did not even provide the accuracy for loss properties. Although, this may be attributed to loss tangent values being too small to accurately measure.

6. Error Analysis

From most of the cited references, it seems safe to conclude that the accuracy of the free-space method is within ±5%. However, this is only an estimation based on a majority of findings, where accuracy and error sources still require much more comprehensive investigations.

It has been recognized that the free-space method is more suitable for broadband measurement of medium and high-loss materials. For materials with loss tangent less than 0.01 the accuracy in loss factor will be worsened, due to inaccurate measurements on reflection and transmission coefficients. Unfortunately, there are many factors that may contribute to errors. In this section, general sources of errors will be discussed without going into too much formulae, which can otherwise be found in references [77, 80, 93].

First, edge diffractions are always harmful to the S-parameters since they cannot really be calibrated. The components of any system have limited size, which inevitably introduce edge diffractions. The edge diffractions take place not only on the focusing elements, but also on the feed horns. A good practice is to place absorbers around the edge of each component, but precautions should be taken so that the presence of absorbers does not disrupt the optical path.

The second factor is Gaussian beam propagation in a free space system. When conducting the line calibration, a distance of L is displaced from its ideal position. Such a displacement introduces extra Gaussian beam phase delay [75], and slight beam divergence. In addition, the presence of the sample plate also modifies the propagation of the Gaussian beam. A good way to mitigate against this is to design the system properly, so that the beam waist at the position of the sample is sufficiently large. By doing so, the plane wave approximation will be sufficiently good, while phase delay and beam divergence will be negligibly small. By the law of a QO system, the best sample size is 4 times that of the beam radius [75]. Therefore, a tradeoff has to be made between the edge diffraction and the Gaussian beam propagation.

System accuracy, stability, and calibration residual error are also important factors. At this stage, the system accuracy and stability can be as good as 0.05 dB/°C for amplitude and 1.1 degree/°C for phase in the mm-wave range. The calibration residual error can be ±0.2 dB for amplitude and ±0.99° for phase (these are typical values of Keysight N5247B). These values contribute to the measurement value by around 1% [77].

Environmental factors such as fluctuating temperature and moisture levels, affects the stability of electronic systems. System error may be minimized if the measurement is conducted in a temperature-controlled room. Now, it is possible to maintain temperature to within ±0.2°C. The effect of moisture may not be significant in the microwave range but needs to be considered in the mm-wave range.

The quality of the beam is very important. Therefore, a corrugated horn is preferred due to its high Gaussianity, good linear polarization, low side lobe and low cross polarization. The drawback is the cost compared with other types of feed horns. Good cross polarization can be obtained, if a small incident angle is used for the free space system [75], which also helps to improve beam quality.

The choice of sample thickness is also critical. In most cases, $\lambda/4$ or $(2n-1)\lambda/4$ is suggested for measurements [36]. Whereas any thickness of multiple half-wavelengths, would not be a good choice for reflection mode. This is because the retrieve from a very small value, often causes much numerical inaccuracy. For a very high-loss sample, the reflection mode is preferred. For medium-lossy sample, the transmission mode may be better. For low-loss samples, this method may not be good enough, where error margins have been quoted as high as 20% in some measurements [62].

To compare the uncertainty of free space and other methods, here particularly transmission line and resonator methods, measured results from the literature have been tabulated in Table III. The accuracy of free space method is referred to Table I and Table II. Since the influential factors/parameters are not exactly the same for these methods, we only present the reported accuracy to the reader. It is seen that the transmission line methods present similar accuracy to the free space methods. Also, they are capable of broadband operation. However, traditional coaxial or waveguide techniques are not so popular in frequencies higher than 110 GHz. The resonator methods provide very good accuracy but are limited to discrete frequencies. For frequencies higher than 300 GHz, the reported data shows much less uncertainty than

seen for lower frequency bands. These findings, imply that the free-space method is competent for broadband measurement in the mm-wave range.

7. Measurement on Metamaterials

The concept of metamaterials was first proposed by Veslago in 1967 [102], and after the pioneering work of Pendry [103] and Shelby et al [104], metamaterials have undergone fast development. From the dielectric point of view, metamaterials are characterized by negative index of permittivity and permeability. Measurement methods were immediately investigated after the first metamaterial was manufactured [105-108], and shortly after extraction methods were derived [109-115].

The uniqueness of metamaterials lies in their non-homogeneous properties. They are built from periodical structures with composite materials. Unlike homogenous media, there is no constant to describe their dielectric property, therefore, the effective permittivity and permeability are used. In addition, metamaterials are dispersive. The effective formulae can be written as [95]

$$\begin{cases} \varepsilon_{\text{eff}}(\omega) = 1 - \dfrac{\omega_p^2}{\omega^2} \\ \mu_{\text{eff}}(\omega) = 1 - \dfrac{F\omega_0^2}{\omega^2 - \omega_0^2 - j\omega\Gamma} \end{cases}, \tag{56}$$

where ω_0, ω_p, Γ and F are parameters relating to the structure and composition of the metamaterial [105]. In consideration of these facts, the measurement of metamaterials has shown some unique properties.

The first theoretical discussion was reported in Ref. [105], where the permittivity was calculated from the constitution relationship between the average electric displacement $\langle D \rangle$ and average electric field $\langle E \rangle$. The method, though theoretically rigorous, requires measurements on electric field and displacement, which is complicated to operate as the electric probe can disturb the original fields in an unpredictable way.

Later, Smith et al reported a method of extracting the dielectric parameters from reflection and transmission coefficients [106]. The method is very similar to the NRW technique. The branch ambiguity issue was noticed in this work, but no specific measures were developed to resolve it. This issue was also discussed by Ziolkowski [108] and a simplified process was proposed, based on the condition of $kd \le 1$

$$\begin{cases} \mu_{\text{eff}}(\omega) = \dfrac{2}{\mathrm{j}k_0 d} \dfrac{1-(S_{21}-S_{11})}{1+(S_{21}-S_{11})} \\ \varepsilon_{\text{eff}}(\omega) = \mu_{\text{eff}}(\omega) + \mathrm{j}\dfrac{2S_{11}}{k_0 d} \end{cases}, \tag{57}$$

where S_{21} and S_{11} are measured transmission and reflection coefficients. It was verified that this set of expressions was valid for several tested samples. The restriction condition of $kd \le 1$ sets a limitation on the upper frequency and introduces extra error that was not discussed.

In Ref. [109], it was argued that the equivalent boundary of a metamaterial was somehow displaced with the physical boundary - a factor that shall be considered when retrieval method is conducted. The equivalent boundaries are optimized by minimizing the impedances of two slabs of metamaterial when they have different thicknesses. After the boundaries are determined, the NRW method shall be applied with the

difference of determined branch. This can be realized by expanding the function $e^{j\sqrt{\varepsilon_{\text{eff}}(f_1)}k_0(f_1)d}$ in a Taylor series:

$$e^{j\sqrt{\varepsilon_{\text{eff}}(f_1)}k_0(f_1)d} = e^{j\sqrt{\varepsilon_{\text{eff}}(f_0)}k_0(f_0)d}\left(1+\Delta+\frac{1}{2}\Delta^2\right) \tag{58}$$

where $\Delta = j\sqrt{\varepsilon_{\text{eff}}(f_1)}k_0(f_1)d - j\sqrt{\varepsilon_{\text{eff}}(f_0)}k_0(f_0)d$, and $k_0(f_0)$ denotes the wave number in free space at frequency f_0. The branch index n is the only unknown. Since the left-handed side of Equation (58) can be determined by the measurement, the Equation (58) is a binominal function of $\sqrt{\varepsilon_{\text{eff}}(f_1)}$. It is seen from Equation (36), the real part can be determined without ambiguity, the correct branch is that the real part of $\sqrt{\varepsilon_{\text{eff}}(f_1)}$ is close to that of $\sqrt{\varepsilon_{\text{eff}}(f_0)}$. This method is very useful for the frequency range out of the resonance. When the frequency approaches the resonance area, this method does not deliver any better than the conventional NRW method. Actually, the value near the resonance is abnormally high, making $\sqrt{\varepsilon_{\text{eff}}(f)}k_0(f)d$ remarkably increased, which makes determination of the branch more difficult.

Numerical methods are also investigated to circumvent the branch issue. In Ref. [110], a genetic algorithm is proposed to retrieve effective parameters of planar metamaterial samples. If the small thickness condition is satisfied, i.e., $\text{Re}(kd) \le 1$, the following relations can be obtained,

$$\begin{cases} \mu_{\text{eff}}(\omega) = \dfrac{2}{jk_0d}\dfrac{1-(S_{21}-S_{11})}{1+(S_{21}-S_{11})} \\ \varepsilon_{\text{eff}}(\omega) = \dfrac{2}{jk_0d}\dfrac{1-(S_{21}+S_{11})}{1+(S_{21}+S_{11})} \end{cases}, \tag{59}$$

which is very similar to Equation (57) and is used to simplify the matching procedure. The dispersion model is chosen to properly characterize the properties of a metamaterial sample. There are a number of models can be used, such as the Lorentz expression, the Debye model, and so forth. However, it should be noted that the curve-fitting method is very much dependent on the assumed medium model, and thus is very likely to cause biased conclusions.

To characterize tensor permittivity and permeability of arbitrary anisotropic metamaterials, a tensor extraction technique was reported [115]. This technique allows all of 18 elements to be nonzero, the extraction is purely based on the given set of measured reflection and transmission coefficients. The incident wave can be decomposed into TE and TM wave, therefore, the transfer matrix contains the information of tensor permittivity and permeability. The extraction formulae are lengthy, and we do not include them in this review. Unfortunately, the method still has the problem of choosing the right branch.

There are still many issues to be addressed in dielectric measurements for metamaterials, such as noise effects, measurement accuracy near resonance, and angular dependence. A good direction is building a robust method based on the NWR method, to provide baseline values in the out of the resonance region and using dielectric models to fit the resonant region. In the process, the sensitivity of electronic instrument may be enhanced to make high permittivity measurements possible.

8. Measurement on Liquids and Gases

The measurements in Table I are mainly for solid samples, but free space mm-wave systems can readily be extended to measure liquid and gas samples. Since both liquids and gases must be contained in an enclosed space, a sample holder usually presents a multilayer structure. Fortunately, the multilayer structure can be analyzed by using the ABCD matrix method or the signal flow method.

For liquid samples, the reflection type of Figure 4(a) and Figure 4(b) can still be used, but the samples need to be fixed horizontally. For Figure 4(c), whilst it is theoretically possible to derive the reflection coefficients, oblique incidence will make the error analysis much more complicated. In this scenario, the reflection of normal incidence may be used as shown in Figure 5, where the system is very similar to the transmission ones.

The transmission systems are also used for liquid samples, as demonstrated in References [54, 69, 71, 116]. By using the methods presented in 3.5, there is no difficulty in retrieving permittivities. It is necessary to know the permittivity of the window material, prior to using these methods. Fortunately, it is very straightforward to measure the permittivity of the window material using the same free space system. In addition, the sample holder can be enclosed in a temperature compartment, enabling temperature dependent characterization, as is similarly described in [117]. Cautions should be taken when high-loss liquid samples are to be measured. For instance, polar molecule liquids normally have very high loss tangent, which in turn requires a wide and dynamic range of mm-wave systems. A way to alleviate this problem is to use a thin sample spacer, so that the transmission loss will be reduced, or alternatively, through the use of a reflection type setup.

For transmission systems at normal incidence (Figure 6, and Figure 8-Figure 14), the ABCD method and the signal flow chart method both provide one with reflection and transmission coefficients. Theoretically, either the reflection or the transmission data can be used for permittivity extraction. However, the reflection and transmission coefficients are both involved in the calculation of permeability and permittivity.

It is not easy to measure the dielectric property of gas in the mm-wave range. This is due to many reasons. One is that gas does not exhibit a fixed form and its permittivity is heavily concentration dependent. More importantly, the permittivity of a gas sample is very close to that of air. Such small differences do not produce reliable changes to the mm-wave signal. In addition, the absorption lines of gases are more observable in the THz range. It is probably due to these reasons that free space measurement on gas samples is rarely reported. By comparison, the free space method used in spectral lines characterization within the THz range, has been used in many cases [118-121].

9. Concluding Remarks

Dielectric measurement is in emergent demand. The accurate extraction of complex dielectric properties is largely based on transmission and reflection measurements. We apologize for not being able to cover every aspect of this area. So far, it seems the free-space method is more suited to medium-loss and high-loss samples. Efforts have been made to make this method applicable to low-loss samples, although no significant progress has been made. We are however optimistic that further improvements of mm-wave free space measurement methods are on the horizon, as new technologies continue to march rapidly forward.

Acknowledgements

This work is supported by the National Natural Science Foundation of China under

the contract number of 61871003, the open project of the state key laboratory of complex electromagnetic environment effects on electronics and information system under grant number CEMEE2021Z0201B, and the Open-ended Foundation of National Radar Signal Processing Laboratory under grant of 61424100105.
Author Contributions: Investigation, Xiaoming Liu, Bin Yang, Lu Gan; Writing – review & editing, Xiaoming Liu, Bin Yang.

Conflicts of Interest: The author declares no conflict of interest.

References

[1] E.-J. Blum, "Radioastronomy at millimeter wavelengths," *Advances in Electronics and Electron Physics*, vol.56, pp.97-162, 1981, doi: 10.1016/S0065-2539(08)60423-0.
[2] A. Gonzalez, K. Kaneko, and S. Asayama, "1.25–1.57 THz dual-polarization receiver optics based on corrugated horns," *IEEE Trans. Thz. Sci. Techn.*, vol. 8, no. 3, pp.321-328, May 2018, doi: 10.1109/TTHZ.2018.2813088.
[3] C. L. Croskey, N. Kämpfer, R. M. Belivacqua, et al, "The millimeter wave atmospheric sounder (MAS): A shuttle-based remote sensing Experiment," *IEEE Trans. Microw. Theory Techn.*, vol. 40, no. 6, pp.1090-1101, June 1992, doi: 10.1109/22.141340.
[4] J. Liu, J. Dai, S. L. Chin and X.-C. Zhang, "Broadband terahertz wave remote sensing using coherent manipulation of fluorescence from asymmetrically ionized gases," *Nature Photonics*, vol. 4, September 2010, pp.627-631, doi: 10.1038/nphoton.2010.165.
[5] B. Williams, "Terahertz quantum-cascade lasers," *Nature Photon*, vol.1, pp.517–525, September 2007, doi: 10.1038/nphoton.2007.166.
[6] D. F. Williams, "500 GHz–750 GHz rectangular-waveguide vector-network-analyzer calibrations," *IEEE Trans. Thz. Sci. Techn.*, vol.1, no.2, pp. 364-377, April 2011, doi: 10.1109/TTHZ.2011.2127370.
[7] T. Merkle, D. Meier, S. Wagner, et al, "Broadband 240-GHz radar for non-destructive testing of composite materials," *IEEE Journal of Solid-State Circuits*, vol.54, no. 9, pp.2388-2401, July 2019, doi: 10.1109/JSSC.2019.2921154.
[8] P. C. Theofanopoulos, M. Sakr, G. C. Trichopoulos, "Multistatic terahertz imaging using the radon transform," *IEEE Trans. Antennas Propag.*, vol. 67, no.4, pp.2700 – 2709, January 2019, doi: 10.1109/TAP.2019.2891461.
[9] L. O. Fhager, S. Heunisch, H. Dahlberg, "Pulsed millimeter wave radar for hand gesture sensing and classification," *IEEE Sensors Letters*, vol.3, no.12, December 2019, Article no. 3502404, doi: 10.1109/LSENS.2019.2953022.
[10] A. Dürr, D. Schwarz, S. Häfner, "High-resolution 160-GHz imaging MIMO radar using MMICs with on-chip frequency synthesizers," *IEEE Trans. Microw. Theory Techn.*, vol.67, no.9, Sept. 2019, pp.3897-3907, doi: 10.1109/TMTT.2019.2906176.
[11] K. A. Smith, C. Csech, D. Murdoch, "Gesture recognition using mm-wave sensor for human-car interface," *IEEE Sensors Letters*, vol. 2, no. 2, June 2018, Article no. 3500904, doi: 10.1109/LSENS.2018.2810093.
[12] Y. Yu, W. Hong, Z.-H. Jiang, "E-band low-profile, wideband 45° linearly polarized slot-loaded patch and its array for millimeter-wave communications, *IEEE Trans. Antennas Propag.*, vol. 66, no.8, Aug. 2018, pp.4364-4369, doi: 10.1109/TAP.2018.2840825.
[13] B. Yang, Z. Yu, R. Zhang, "Local oscillator phase shifting and harmonic mixing-based high-precision phased array for 5G millimeter-wave communications," *IEEE Trans. Microw. Theory Techn.*, vol. 67, no. 7, July 2019, pp.3162-3173, doi: 10.1109/TMTT.2019.2899598.
[14] B. Yang, Z. Yu, J. Lan, "Digital beamforming-based massive MIMO transceiver for 5G millimeter-wave communications," *IEEE Trans. Microw. Theory Techn.*, vol. 66, no. 7, July 2018, pp.3403-3418, doi: 10.1109/TMTT.2018.2829702.
[15] D. M. Sheen, D. L. Mcmakin, T. E. Hall, "Three-dimensional millimeter-wave imaging for concealed weapon detection," *IEEE Trans. Microw. Theory Techn.*, vol. 49, no. 9, pp.1581-1592, Sept 2001, doi: 10.1109/22.942570.
[16] C. A. Balanis, "Advanced Engineering Electromagnetics 2nd edition," New York, USA, Wiley, 2012.
[17] S. Baba, I. Mori, T. Nakano, "Precise determination of the refractive index of sputtered MgO thin films in the visible light range," *Vacuum*, vol.59, no. 2-3, pp.531-537, November 2000, doi: 10.1016/S0042-207X(00)00312-2.
[18] A. I. Sulyman, A. M. T. Nassar, M. K. Samimi,et al, "Radio propagation path loss models for 5G cellular networks in the 28 GHz and 38 GHz millimeter-wave bands," *IEEE Commun. Mag.*, vol.52, no. 9, pp.78-86, September 2014, doi: 10.1109/MCOM.2014.6894456.
[19] N. Ito, A. Mase, Y. Kogi, N. Seko, et al, "New advanced fabrication technique for millimeter-wave planar components based on fluororesin substrates using graft polymerization," *Japanese Journal of Applied Physics*, vol.47, no.6, pp.4755–4758, 2008, doi:10.1143/jjap.47.4755.
[20] W. C. Yang, H. Wang, W. Q. Che, et al, "High-gain and low-loss millimeter-wave LTCC antenna array using artificial magnetic conductor structure," *IEEE Trans. Antennas and Propag.*, vol.63, no.1, pp.390–395, Jan 2015, doi:10.1109/tap.2014.2364591.
[21] N. W. B. Stone, J. E. Harries, D. W. E. Fuller, et al. Electrical standards of measurement. Part 3: Submillimetre-wave measurements and standards," *Proceedings of the Institution of Electrical Engineers*, vol.122, no.10, pp.1054-1070, October 1975, doi: 10.1049/piee.1975.0264.
[22] M. N. Afsar, J. Chamberlain, G. W. Chantry, "High-precision dielectric measurements on liquids and solids at millimeter and submillimeter wavelengths," *IEEE Trans. Instru. Meas.*, vol. 25, no.4, pp.290-294, Dec 1976, doi: 10.1109/TIM.1976.6312229.
[23] M. J. Bangham, J. R. Birch, T. G. Blaney, et al, Physical measurement in the 100–1000 GHz frequency range. *Radio and Electronic Engineer*, vol.49, no.7-8, pp.403-418, July-August 1979, doi:10.1049/ree.1979.0074.
[24] U. Kaatze, "Measuring the dielectric properties of materials. Ninety-year development from low-frequency techniques to broadband spectroscopy and high-frequency imaging," *Measurement Science and Technology*, vol.24, no.1, Article no. 012005, December 2013, doi: 10.1088/0957-0233/24/1/012005.

[25] R. N. Clarke and C. B. Rosenberg.Fabry-Perot and open resonators at microwave and millimetre wave frequencies, 2-300GHz. *J. Phys. E: Sci. Instrum.* vol.15, no.1, pp.9-24, November, 1982, doi: 10.1088/0022-3735/15/1/002.
[26] H. A. Resing and R. A. Neihof. Nuclear magnetic resonance relaxation of water adsorbed on bacterial cell walls. *Journal of Colloid and Interface, Science*, vol, 34, no. 4, pp.480-487, December 1970, doi: 10.1016/0021-9797(70)90209-2.
[27] T. E.Talpey, Optical methods for the measurement of complex dielectric and magnetic constants at centimeter and millimeter wavelengths," *Transactions of the IRE Professional Group on Microwave Theory and Techniques*, vol. 2, no.3, pp.1-12, September 1954, doi: 10.1109/TMTT.1954.1124880.
[28] K. H. Breeden, "Error analysis for waveguide-bridge dielectric-constant measurements at millimeter wavelengths," *IEEE Trans. Instru. Meas.*, vol.18, no.3, pp.203-208, September 1969, doi: 10.1109/TIM.1969.4313801.
[29] C. K. Campbell, "Free-space permittivity measurements on dielectric materials at millimeter wavelengths," *IEEE Trans. Instru. Meas.*, vol.27, no.1, pp.54-58, March 1978, doi: 10.1109/TIM.1978.4314617.
[30] P. K. Kadaba, "Simultaneous measurement of complex permittivity and permeability in the millimeter region by a frequency-domain technique," *IEEE Trans. Instru. Meas.*, vol.33, no.4, pp.336-340, 1984, doi: 10.1109/TIM.1984.4315236.
[31] F. I. Shimabukuro, S. Lazar, M. R. Chernick M R, et al, "A quasi-optical method for measuring the complex permittivity of materials," *IEEE Trans. Microw. Theory Techn.*, vol.32, no.7, pp.659-665, July 1984, doi: 10.1109/TMTT.1984.1132750.
[32] J. Joseph, R. Jost, E. Utt, "Mutiple angle of incidence measurement technique for the permittivity and permeability of lossy materials at millimeter wavelengths," In *Proc. 1987 Antennas and Propagation Society International Symposium*, Blacksburg, VA, USA, June 1987, pp.640-643.
[33] A. L. Cullen, "A new free-wave method for ferrite measurement at millimeter wavelengths," *Radio Science*, vol. 22, no. 7, pp. 1168-1170, December 1987, doi: 10.1029/RS022i007p01168.
[34] D. K. Ghodgaonkar, V. V. Varadan, V. K. Varadan, "A free-space method for measurement of dielectric constants and loss tangents at microwave frequencies," *IEEE Trans. Instru. Meas.*, vol.38, no.3, pp. 789-793, Jun 1989, doi: 10.1109/19.32194.
[35] D. K. Ghodgaonkar, V. V. Varadan, V. K. Varadan, "Free-space measurement of complex permittivity and complex permeability of magnetic materials at microwave frequencies, " *IEEE Trans. Instru. Meas.*, vol.39, no.2, pp.387-394, April 1990, doi: 10.1109/19.52520.
[36] A. C. Lynch, D. Simkin, "Measurement of permeability and permittivity of ferrites," *Measurement Science & Technology*, vol.1, no.11, pp.1162-1167, November, 1990, doi: 10.1088/0957-0233/1/11/006.
[37] A. C. Lynch, H. D. Griffiths, S. Appleton, "Free-wave measurement of permeability and permittivity of ferrites at millimetre-wave frequencies," *IEE Proc.-Sci. Meas. Technol.*, vol.142, no.2, pp.169-175, 1995, doi: 10.1049/ip-smt:19951691.
[38] G. L. Friedsam, E. M. Biebl, "A broadband free-space dielectric properties measurement system at millimeter wavelengths," *IEEE Trans. Instru. Meas.*, vol.46, no.2, pp.515-518, April 1997, doi: 10.1109/19.571899.
[39] J. Munoz, M. Rojo, A. Parrefio, "Automatic measurement of permittivity and permeability at microwave frequencies using normal and oblique free-wave incidence with focused beam," *IEEE Trans. Instru. Meas.*, vol.47, no.4, pp.886-892, August 1998, doi: 10.1109/19.744638.
[40] M. Le Goff, J. L. Le Bras, B. Deschamps, et al, "Ka Band Quasi Optical Test Bench using Focusing Horns," in *Proc. 29th European Microwave Conference*, Munich, Germany, October 1999, pp.240-243.
[41] S. B. Kumar, U. Raveendranath, P. Mohanan, et al. "A simple free-space method for measuring the complex permittivity of single and compound dielectric materials," *Microwave and Optical Technology Letters*, vol.26, no.2, pp.117-119, July 2000, doi: 10.1002/1098-2760(20000720)26:2<100::AID-MOP10>3.0.CO;2-I.
[42] R. D. Hollinger, K. A. Jose, A. Tellakula, "Microwave characterization of dielectric materials from 8 to 110 GHz using a free pace setup," *Microwave & Optical Technology Letters*, vol.26, no.2, pp.100-105, July 2000, doi: 10.1002/1098-2760(20000720)26:2<100::AID-MOP10>3.0.CO;2-3.
[43] N. Gagnon, J. Shaker, P. Berini, et al, "Material characterization using a quasi-optical measurement system," *IEEE Trans. Instru. Meas.*, vol.52, no.2, pp.333-336, April 2003, doi: 10.1109/TIM.2003.810042.
[44] N. Gagnon, J. Shaker, L. Roy, et al, "Low-cost free-space measurement of dielectric constant at Ka band," *IEE Proceedings-Microwaves, Antennas and Propagation*, vol.151, no.3, pp.271-276, June 2004, doi: 10.1049/ip-map:20040264.
[45] N. Gagnon, J. Shaker, "Accurate phase measurement of passive non-reciprocal quasi-optical components," *IEE Proceedings-Microwaves, Antennas and Propagation*, vol.152, no.2, pp.111-116, April 2005, doi: 10.1049/ip-map:20045029.
[46] D. Bourreau, A. Peden, S. L. Maguer, "A quasi-optical free-space measurement setup without time-domain gating for material characterization in the w-band," *IEEE Trans. Instru. Meas.*, vol.55, no.6, pp.2022-2028, December 2006, doi: 10.1109/TIM.2006.884283.
[47] A. Elhawil, L. Zhang, J. Stiens, et al, "A Quasi-Optical Free-Space Method for Dielectric Constant Characterization of Polymer Materials in mm-wave Band" in *Proc. Proceedings Symposium IEEE/LEOS Benelux Chapter*, 2007, Brussels, pp.187-190.
[48] F. H. Wee, P. J. Soh, A. H. M. Suhaizal, et al, "Free Space Measurement Technique on Dielectric Properties of Agricultural Residues at Microwave Frequencies," in Proc. 2009 SBMO/IEEE MTT-S International Microwave and Optoelectronics Conference (IMOC), Belem, Brazil, March 2009.
[49] S. Chen, K. A. Korolev, J. Kupershmidt, et al, "High-resolution high-power quasi-optical free-space spectrometer for dielectric and magnetic measurements in millimeter waves," *IEEE Trans. Instru. Meas.*, vol.58, no.8, pp.2671-2678, August 2009, doi: 10.1109/TIM.2009.2015699.
[50] J. R. Peacock, "Millimetre wave permittivity of water near 25˚C," *J. Phys. D: Appl. Phys.*, vol.42, article no. 205501, September 2009, doi:10.1088/0022-3727/42/20/205501.
[51] B. Yang, R. J. Wylde, D. H. Martin, et al, "Determination of the Gyrotropic characteristics of hexaferrite ceramics from 75 to 600 GHz," *IEEE Trans. Microw. Theory Techn.*, vol. 58, no. 12, pp. 3587-3597, December 2010, doi: 10.1109/TMTT.2010.2086290.
[52] F. Zaki, Z. Awang, "A free-space method for measurement of complex permittivity of double-layer dielectric materials at microwave frequencies," In Proc. 2010 IEEE Student Conference on Research and Development (SCOReD), Putrajaya, Malaysia, December 2010, pp.12-15.
[53] B. Maffei, S. Legg, M. Robinson, et al, "Implementation of a quasi-optical free-space s-parameters measurement system," in Proc. 35th ESA Antenna Workshop on Antenna & Free Space RF Measurements, Noordwijk, The Netherlands, January 2013.
[54] X. Liu, H.-J. Chen, B. Yang, et al, "Dielectric property measurement of gold nanoparticle dispersions in the millimeter wave range," *Journal of Infrared Millimeter & Terahertz Waves*, vol. 34, no.2, pp. 140-151, February 2013, doi: 10.1007/s10762-013-9957-7.

[55] A. Kazemipour, M. Hudlicka, M. Salhi, et al, "Free-space quasi-optical spectrometer for material characterization in the 50-500 GHz frequency range," in Proc. of the 44th European Microwave Conference, Rome Italy, October 2014, pp.636-639.
[56] A. Kazemipour, M. Hudlička, S. K. Yee, et al, "Design and calibration of a compact quasi-optical system for material characterization in millimeter/submillimeter wave domain," *IEEE Trans. Instru. Meas.*, vol.64, no.6, pp.1438-1445, July 2015, doi: 0.1109/TIM.2014.2376115.
[57] T. Tosaka, K. Fujii, K. Fukunaga, et al, "Development of complex relative permittivity measurement system based on free-space in 220–330 GHz range," *IEEE Trans. Thz. Sci. Techn.*, vol.5, no.1, pp.102-109, January 2015, doi: 10.1109/TTHZ.2014.2362013.
[58] X. Zhang, T. Chang, H. L. Cui, et al, "A free-space measurement technique of terahertz dielectric properties," *Journal of Infrared, Millimeter, and Terahertz Waves*, vol. 38, pp.3, pp.356-365, March 2016, doi: 10.1007/s10762-016-0341-2.
[59] A. M. Hassan, J. Obrzut, E. J. Garboczi, "A Q-band free-space characterization of carbon nanotube composites," *IEEE Trans. Microw. Theory Techn.*, vol.64, no.11, pp.3807-3819, November 2016, doi: 10.1109/TMTT.2016.2603500.
[60] J. Hammler, A. J. Gallant, C. Balocco, "Free-space permittivity measurement at terahertz frequencies with a vector network analyzer," *IEEE Trans. Thz. Sci. Techn.*, vol.6, no.6, pp.817-823, July 2016, doi: 10.1109/TTHZ.2016.2609204.
[61] Y.-P. Hong, D.-J. Lee, M. J. Salter, "Broadband measurement of high permittivity at millimetre-wave frequencies," *Electronics Letters*, vol.52, no.9, pp.725–727, September 2016, doi:10.1049/el.2015.3886.
[62] Z. Akhter, M. J. Akhtar, "Free-space time domain position insensitive technique for simultaneous measurement of complex permittivity and thickness of lossy dielectric samples," *IEEE Trans. Instru. Meas.*, vol.65, no.10, pp.2394-2405, October 2016, doi: 10.1109/TIM.2016.2581398.
[63] T. Horák, G. Ducournau, M. Mičica, et al, "Free-space characterization of magneto-optical hexaferrites in the submillimeter-wave range," *IEEE Trans. Thz. Sci. Techn.*, vol.7, no.5, pp.563-571, September 2017, doi: 10.1109/TTHZ.2017.2736340.
[64] T. Ozturk, M. Hudlička, İ. Uluer, "Development of Measurement and Extraction Technique of Complex Permittivity Using Transmission Parameter S21 for Millimeter Wave Frequencies," *Journal of Infrared Millimeter & Terahertz Waves*, vol. 38, pp.1510–1520, July 2017, doi: 10.1007/s10762-017-0421-y.
[65] T. Chang, X. Zhang, C. Yang, et al, "Measurement of complex terahertz dielectric properties of polymers using an improved free-space technique," *Measurement Science and Technology*, vol. 28, vol.4, article no.045002, January 2017, doi: 10.1088/1361-6501/aa58b5.
[66] P. R. Smith, J. C. Weatherall, J. Barber, et al, "Measurements of the dielectric properties of explosives and inert materials at millimeter wave frequencies (V-band and above) using free space reflection methods," Proc. SPIE 10189, Passive and Active Millimeter-Wave Imaging XX, 1018908, May 2017, doi: 10.1117/12.2267195.
[67] A. Rasidian, L. Shafai, D. Klymyshyn, et al. "A fast and efficient free-space dielectric measurement technique at mm-wave frequencies," *IEEE Antennas & Wireless Propagation Letters*, vol.16, pp. 2630-2633, August 2017, doi: 10.1109/LAWP.2017.2737632.
[68] E. Hajisaeid, A. F. Dericioglu, A. Akyurtlu, Alkim, "All 3-D printed free-space setup for microwave dielectric characterization of materials," *IEEE Trans. Instru. Meas.*, vol.67, no.8, pp. 1877-1886, March 2018, doi: 10.1109/TIM.2018.2805962.
[69] X. Liu, J. Yu, X. Chen, et al, "A broadband quasi-optical system for measuring the dielectric properties in the terahertz band," Journal of Radars, vol.7, no.1, pp.56–66, January, 2018 (in Chinese), DOI:10.12000/JR17110.
[70] X. Yang, X. Liu, S. Yu, et al, "Permittivity of Undoped Silicon in the Millimeter Wave Range," Electronics, vol. 8, no. article no. 886, Auguest 2019, doi:10.3390/electronics8080886.
[71] X. Liu, J. Yu, "Characterization of the dielectric properties of water and methanol in the D-band using a quasi-optical spectroscopy," Scientific Reports, vol. 9, article no.18562, December 2019, doi:10.1038/s41598-019-55126-6.
[72] M. S. Hilario, B. W. Hoff, B. Jawdat, et al, "W-band complex permittivity measurements at high temperature using free-space methods," *IEEE Transactions on Components, Packaging and Manufacturing Technology*, vol.9, no.6, pp. 1011-1019, April 2019, doi: 10.1109/tcpmt.2019.2912837.
[73] A. M. Nicolson, and G. F. Ross, "Measurement of the intrinsic properties of materials by time domain techniques," *IEEE Trans. Instru. Meas.*, vol.19, no.4, pp. 377-382, November 1970, doi: 10.1109/TIM.1970.4313932.
[74] W. B. Weir, "Automatic measurement of complex dielectric constant and permeability at microwave frequencies," *Proceedings of the IEEE*, vol.62, no.1, pp. 33-36, January 1974, doi: 0.1109/PROC.1974.9382.
[75] P. F. Goldsmith, "Quasioptical Systems: Gaussian Beam Quasioptical Propogation and Applications," New York, Wiley-IEEE Press, 1998.
[76] D. Fasold, "Measurement performance of basic compact range concepts," International Symposium on Antenna and RCS Measurement Techniques, Munich, Germany, May 2006.
[77] A. H. Boughriet, C. Legrand, A. Chapoton, "Noniterative stable transmission/reflection method for low-loss material complex permittivity determination," *IEEE Transactions on Microwave Theory and Techniques*, vol.45, no.1, pp. 52-57, January 1997, doi: 10.1109/22.552032.
[78] S. S. Stuchly, M. Matuszewski, "A combined total reflection-transmission method in application to dielectric spectroscopy," *IEEE Trans. Instru. Meas.*, vol.27, no.3, pp. 285-288, September 1978, doi: 10.1109/TIM.1978.4314682.
[79] L. P. Ligthart, "A fast computational technique for accurate permittivity determination using transmission line methods," *IEEE Trans. Microw. Theory Techn.*, vol.31, no.3, pp. 249-254, March 1983, doi: 10.1109/TMTT.1983.1131471.
[80] J. Baker-Jarvis, E. J. Vanzura, W. A. Kissick, "Improved technique for determining complex permittivity with the transmission/reflection method," *IEEE Trans. Microw. Theory Techn.*, vol.38, no.8, pp. 1096-1103, August 1990, doi: 10.1109/22.57336.
[81] D. W. Marquardt, "An algorithm for least-squares estimation of nonlinear parameters," *J. Soc. Ind, Appl. Math.*, vol.11, no.2, pp. 431-441, June 1963, doi: 10.2307/2098941.
[82] W. Wiesbeck, D. Kahny, "Single reference, three target calibration and error correction for monostatic, polarimetric free space measurements," *Proceedings of the IEEE*, vol.79, no.10, pp. 1551-1558, October 1991, doi: 10.1109/5.104229.
[83] F. C. Smith, B. Chambers, J. C. Bennett, "Calibration techniques for free space reflection coefficient measurements," *IEE Proceedings-A*, vol.139, no.5, pp. 247-253, September 1992, doi: 10.1049/ip-a-3.1992.0043.
[84] N. Gagnon, J. Shaker, P. Berini, et al, "Correction and Extraction Techniques for Dielectric Constant Determination Using a Ka-Band Free-Space Measurement System," in Proc. European Microwave Conference 2002, Milan, Italy, September, 2002.
[85] I. Rolfes, B. Schiek, "Calibration Methods for Free Space Dielectric Microwave Measurements with a 4-Channel-Network-Analyzer," 32nd European Microwave Conference, Milan, Italy, 2002.

[86] S. Trabelsi, S. O. Nelson, A. W. Kraszewski, "Calibrating free-space measurement systems for microwave moisture sensing in granular materials," IMTC/2002. Proceedings of the 19th IEEE Instrumentation and Measurement Technology Conference (IEEE Cat. No.00CH37276), Anchorage, AK, USA, May 2002.
[87] I. Rolfes, B. Schiek, "Calibration methods for microwave free space measurements," *Advances in Radio Science*, vol.2, pp. 19-25, January 2004, doi: 10.5194/ars-2-19-2004.
[88] P. G. Bartley, S. B. Begley, "Improved free-space S-parameter calibration," 2005 IEEE Instrumentationand Measurement Technology Conference Proceedings, Ottawa, Canada, May 2005.
[89] U. C. Hasar, O. Simsek, "A calibration-independent microwave method for position-insensitive and nonsingular dielectric measurements of solid materials," *Journal of Physics D: Applied Physics*, vol.42, no.7, article no. 075403, March 2009, doi: 10.1088/0022-3727/42/7/075403. (10 pp).
[90] P. G. Bartley, S. B. Begley, "A new free-space calibration technique for materials measurement," 2012 IEEE Instrumentation & Measurement Technology Conference, Graz, Austria, May 2012.
[91] J. P. Dunsmore, "Handbook of Microwave Component Measurements with advanced VNA techniques," New York, Wiley Press, 2012.
[92] Y. Satoa, N. Oguraa, Y. Yamaguchia, et al, "Development of a sensor for dielectric constant measurements utilizing time-domain measurement with a vector network analyzer," *Measurement*, vol. 169, paper ID:108530, February 2021, doi:10.1016/j.measurement.2020.108530.
[93] L. Cerulloa, J. Wingesa, T. Rylandera, et al, "Microwave measurement system for dispersive dielectric properties of densely packed pellets," *Measurement*, vol. 106, pp.179-189, August 2017, doi:10.1016/j.measurement.2017.03.013.
[94] Z. Abbas, R. D. Pollard, and R. W. Kelsall, "Determination of the dielectric constant of materials from effective refractive index measurements," *IEEE Trans. Instru. Meas.*, vol. 47, no. 1, pp.148-152, February 1998.
[95] Z. Abbas, R. D. Pollard, and R. W. Kelsall, "A rectangular dielectric waveguide technique for determination of permittivity of materials at W-band," *IEEE Trans. Microw. Theory Techn.*, vol.6, no.12, pp.2011-2015, 2002, doi: 10.1109/22.739275.
[96] M. D. Janezic, D. F. Williams, V. Blaschke, et al, "Permittivity characterization of low-k thin films from transmission-line measurements," *IEEE Trans. Microw. Theory Techn.*, vol. 51, no. 1, pp.132-136, January 2003, doi: 10.1109/TMTT.2002.806925.
[97] J. Degenford, P. Coleman, "A quasi-optics perturbation technique for measuring dielectric constants," *Proceedings of the IEEE*, vol.54, no.4, pp.520–522, April 1966, doi:10.1109/PROC.1966.4767
[98] K. H. Breeden, J. B. Langley, "Fabry-Perot cavity for dielectric measurements," *Review of Scientific Instruments*, vol.40, no.9, pp.1162-1163, September 1969, doi: 10.1063/1.1684188.
[99] A. C. Lynch, "Measurement of permittivity by means of an open resonator. II. Experimental. *Proc. R. Soc. Lond. A*, vol.380, pp.73-76, March 1982, doi: 10.1098/rspa.1982.0030.
[100] M. N. Afsar, H. Ding, and K. Tourshan, "A new 60 GHz open-resonator technique for precision permittivity and loss-tangent measurement," *IEEE Trans. Instru. Meas.*, vol. 48, no. 2, pp.626-630, April 1999, doi: 10.1109/19.769673.
[101] S. Chen and M. N. Afsar, "Fabry–Perot open resonator technique for dielectric permittivity and loss tangent measurements of Yttrium Iron Garnet," *IEEE Trans. Magnet.*, vol. 43, no. 6, pp.2734-2736, June 2007, doi:10.1109/TMAG.2007.892855.
[102] V. G. Veselago, "The electrodynamics of substances with simultaneously negative values of ε and μ," *Physics-Uspekhi*, vol. 10, no. 4, pp. 509–514, 1968, doi: 10.1070/PU1968v010n04ABEH003699.
[103] J. B. Pendry, A. J. Holden, D. Robbins, et al, "Magnetism from conductors and enhanced nonlinear phenomena," *IEEE Trans. Microw. Theory Tech.*, vol. 47, no. 11, pp. 2075–2084, Nov. 1999, doi: 10.1109/22.798002.
[104] R. A. Shelby, D. R. Smith, and S. Schultz, "Experimental verification of a negative index of refraction," *Science*, vol. 292, no. 5514, pp. 77–79, Apr. 2001, doi: 10.1126/science.1058847.
[105] D. R. Smith, D. C. Vier, N. Kroll, et al, "Direct calculation of permeability and permittivity for a left-handed metamaterial," *Applied Physics Letters*, vol.77, no.14, pp. 2246-2248, October 2000, doi: 10.1063/1.1314884.
[106] D. R. Smith and S. Schultz, "Determination of effective permittivity and permeability of metamaterials from reflection and transmission coefficients," *Physical Review B*, vol.65, no.19, article no. 195104, November 2002, doi: 10.1103/PhysRevB.65.195104.
[107] P. Markoš, C. M. Soukoulis, "Transmission properties and effective electromagnetic parameters of double negative metamaterials," Optics Express, vol. 11, no.7, pp.649-661, May 2003, doi: 10.1364/OE.11.000649.
[108] R. W. Ziolkowski, "Design, fabrication, and testing of double negative metamaterials," *IEEE Trans. Antennas and Propag.*, vol.51, no.7, pp.1516-1529, July 2003 doi: 10.1109/TAP.2003.813622.
[109] X. Chen, T. M. Grzegorczyk, B.-I. Wu,et al, "Robust method to retrieve the constitutive effective parameters of metamaterials," *Physical Review E*, vol.70, article no. 016608, July 2004, doi: 10.1103/PhysRevE.70.016608.
[110] S. Tricarico, F. Bilotti, and . Vegni, "A genetic algorithm based procedure to retrieve effective parameters of planar metamaterial samples," *Proc. of SPIE*, vol. 7353, article no. 73530H-1, May 2009, doi: 10.1117/12.820648.
[111] V. Tyagi and E. Semouchkina, "Sensitivity analysis of the effective parameter extraction procedure for metamaterial applications," *Microwave and Optical Technology Letters*, vol. 51, no. 4, pp. 1013-1017, April 2009, doi:10.1002/mop.24267.
[112] D. H. Lee and W. S. Park, "Extraction of effective permittivity and permeability of periodic metamaterial cells, *Microwave and Optical Technology Letters*, vol. 51, no. 8, pp.1824-1830, August 2009, doi:10.1002/mop.24468.
[113] S. Kim, E. F. Kuester, C L. Holloway,Et al, "Boundary effects on the determination of metamaterial parameters from normal incidence reflection and transmission measurements," *IEEE Trans. Antennas and Propag.*, vol. 59, no. 6, pp.2226-2240, June 2011, doi: 10.1109/TAP.2011.2143679.
[114] L. Chen, Z. Lei, R. Yang, Et al, "Determining the effective electromagnetic parameters of bianisotropic metamaterials with periodic structures," *Progress in Electromagnetics Research M*, vol. 29, pp.79-93, January 2013, doi: 10.2528/PIERM13010204.
[115] M. R. Benson, A. G. Knisely, M. A. Marciniak, et al, "Permittivity and permeability tensor extraction technique for arbitrary anisotropic materials," *IEEE Photonics Journal*, vol. 7, no. 3, article no. 2600613, June 2015, doi: 10.1109/JPHOT.2015.2440759.
[116] A. K. Fahd and P. G. Steffes, "Laboratory mesurement of the millimeter wave properties of liquid sulfuric acid (H2SO4)," *Journal of Geophysical Research*, vol.96, no. E2, pp.17471-17476, September, 1991, doi: 10.1029/91JE01684.
[117] X. Liu, S. Yu, L. Gan, et al, "Broadband quasi-optical dielectric spectroscopy for solid and liquid samples," Journal of Infrared, Millimeter, and Terahertz Waves, vol. 41, pp. 810–824, June 2020, doi: 10.1007/s10762-020-00710-5.
[118] S. A. Harmon, R. A. Cheville, "Part-per-million gas detection from long-baseline THz spectroscopy," *Applied Physics Letters*, vol.85, no.11, pp. 2128-2130, September 2004, doi: 10.1063/1.1788896.

[119] N. Rothbart, O. Holz, R. Koczulla, et al, “Analysis of human breath by millimeter-wave/terahertz spectroscopy,” *Sensors*, vol.19, no.12, article no. 2719, June 2019, doi: 10.3390/s19122719
[120] C. F. Neese, I. R. Medvedev, G. M. Plummer, et al, “Compact submillimeter/terahertz gas sensor with efficient gas collection, preconcentration, and ppt sensitivity,” *IEEE Sensors Journal*, vol.12, no.8, pp. 2565-2574, April 2012, doi: 10.1109/JSEN.2012.2195487.
[121] N. Rothbart, K. Schmalz, and H.-W. Hübers, “A compact circular multipass cell for millimeter-wave/terahertz gas spectroscopy,” *IEEE Trans. Thz. Sci. Techn.*, vol.10, no.1, pp. 9-14, October 2019, doi: 10.1109/TTHZ.2019.2950123.

Table I Key features of the free-space measurement systems in the literature

Ref.	System configuration	Freq. (GHz)	Sample	Calibration	Extraction Method	Parameters	Accuracy
[27-29]	Reflection arc, also in transmission mode	35	Solid	Reference measurement using a metal	Using the Brewster angle formula	ε_r, μ_r	< ±5.0%
[30]	Horn to horn with phase locked electronic system, in transmission mode	56, 94	Solid	Reference measurement using a shorting metal	Theoretical formulae	ε_r, μ_r	-
[31],[32]	Horn to horn with phase locked electronic system, in transmission mode	94	Solid	-	Numerical best-fit estimates	ε_r	±0.2%
[33]	Horn to horn, reflection type with sample backed by a metallic plate	-	Solid	Reference measurement using a metal	Theoretical formulae	ε_r, μ_r	-
[34]	Horn with spot-focusing lens, in reflection mode	14.5-17.5	Solid	TRL + time-domain gating	Theoretical formulae	ε_r	±0.2%
[35]	Horn with spot-focusing lens, in transmission mode	8.2-40	Solid	TRL + time-domain gating	Theoretical formulae	ε_r, μ_r	< ±5.0%
[36]	Horn to horn, reflection type with sample backed by a metallic plate	35	Solid	Reference measurement using a metal	Theoretical formulae	ε_r, μ_r	-
[37]	Horn with ellipsoidal and spherical mirrors, in both transmission and reflection modes	10-40	Solid	Reference measurement using a metal (or open path) + time-domain gating	Theoretical formulae	ε_r, μ_r	±5.0%
[38]	Horn with one lens on the transmitting side, in transmission mode	75-95	Solid	time-domain gating	Nonlinear least-squares method	ε_r	2.3%
[39]	Horn with one ellipsoidal on the transmitting side, in transmission mode	9.5-11.5	Solid	TRL + time-domain gating	Multi-angle technique	ε_r, μ_r	Average 5%
[40]	Horn with spot-focusing lens, in transmission mode	75-110	Solid	TRL calibration	-	ε_r	-
[41]	Horn to horn in transmission mode	8-12	Solid	TRL calibration	Theoretical formulae	ε_r	4%
[42]	Horn with spot-focusing lens, in transmission mode	10-110	Solid	TRL calibration	Theoretical formulae	ε_r	-
[43-45]	Horn with spot-focusing lens, in transmission mode	28-32	Solid	TRM calibration	Root-finding algorithm Genetic algorithm	ε_r	2.5%
[46]	Horn with spot-focusing lens, in transmission mode	75-110	Solid	TRL calibration	Numerical calculation from error function	ε_r	-
[47]	Four-mirror quasi-optical system	75-110	Solid	Reference measurement on baseline	Genetic algorithm	ε_r	-
[48]	Horn to horn in transmission mode	2.2-3.3	Solid	SLOT + time-domain gating Agilent 85071E	Theoretical formulae	ε_r	-
[49]	Horn with spot-focusing lens, in transmission mode	60-90	Solid	Reference measurement on baseline	Numerical fitting	ε_r, μ_r	1.0%
[50]	Horn with spot-focusing lens, in reflection mode	75-110	Liquid	Reference measurement on baseline and metal reflection	Numerical fitting	ε_r	-
[51]	Quasi-optical system, horn with focusing reflectors and polarizers	75-600	Solid	Reference measurement on baseline	Numerical fitting	ε_r	-
[52]	Quasi-optical system, horn with focusing reflectors and polarizers	18-26	Solid	LRL + time-domain gating	Theoretical formulae	ε_r	-
[53]	Quasi-optical system, dual CTR	75-110	Solid	TRL calibration	-	ε_r	1.0%
[54]	Quasi-optical system, horn with focusing reflectors and polarizers	75-110	Solid, liquid	Reference measurement on baseline	Numerical extraction	ε_r	±5.0%
[55-56]	Horn with off-axis parabolic mirrors	50-500	Solid	TRM up to 100GHz, TRL for higher frequency. Reference measurement on baseline.	Theoretical formulae	ε_r	1.0%-2.0%
[57]	Horn with spot-focusing lens, in transmission mode	220-300	Solid	TRL calibration	Numerical extraction	ε_r	10%
[58]	Horn with spot-focusing lens, in transmission mode	325-500	Solid	Full two port VNA calibration + TRL calibration	Nicolson-Ross-Weir algorithm	ε_r	±5.0%
[59]	Horn to horn in transmission mode	30-50	Solid	LR + time gating	Nicolson-Ross-Weir algorithm	ε_r	±2.0%

[60]	Horn with focusing reflectors, in transmission mode	750-1100	Solid	Reference measurement on baseline + de-embedding process	Monte Carlo simulation	ε_r	-
[61]	Horn with focusing reflectors, in transmission mode	220-330	Solid	TRL calibration	Numerical extraction	ε_r	±2.0%
[62]	Horn to horn in transmission mode	26.5-40	Solid	No calibration required	Smart variable update with binary decision tree	ε_r	±4.0%
[63]	Horn with 4 focusing reflectors, in transmission mode	325-500	Solid	Reference measurements on baseline and metal reflection	Least-squares data fit	ε_r, μ_r	-
[64]	Horn with off-axis parabolic mirrors	325-500	Solid	Reference measurements on baseline	Numerical extraction	ε_r	±4.0%
[65]	Horn to horn	325-500	Solid	GRL calibration	Newton iterative method	ε_r	±5.0%
[66]	Horn with reflection plate	60-90	Solid	Reference measurements on metal reflection	Numerical fitting of reflection data	ε_r	-
[67]	Horn to horn	50-51	Solid	SLOT VNA calibration + TRM free-space calibration	Zero-finding technique	ε_r	<±4.0%
[68]	Horn with focusing lens, in transmission mode (3D printing fabrication)	2-18	Solid	TRL calibration	Nicolson-Ross-Weir algorithm	ε_r, μ_r	<±4.0%
[69]	Horn with focusing reflectors, in transmission mode	110-170	Solid, liquid	Reference measurement on baseline	Numerical extraction	ε_r	±5.0%
[70]	Horn with focusing reflectors, in transmission mode	60-90	Solid	Reference measurement on baseline	Numerical extraction	ε_r	±5.0%
[71]	Quasi-optical system, horn with focusing reflectors and polarizers	140-170	Solid, liquid	Reference measurement on baseline	Numerical extraction	ε_r	±5.0%
[72]	Horn with spot-focusing lens, in transmission mode (For high temperature measurement)	75-110	Solid	TRL+GRL calibration	Least-squares fitting	ε_r	±0.5%

Table II The measured results using free space methods in the literature

Ref	Freq/GHz	Material	ε_r	Tanδ	$\Delta\varepsilon_r$ (%)	Δtanδ (%)
[27]	35.9	Bakelite	3.85	0.0526	±6.0%	-
		Glass	7.24	0.0234		
		Polystyrene	2.52	0.0092		
		Paraffin	2.54	-		
[28]	94	Fused silica	3.216	0.0026	-	-
[29]	35	Bakelite	3.85	0.050	±5.0%	-
		Polymethyl methacrylate	2.45	0.002		
		96% Alumina	8.68	0.008		
[30]	56	Plexiglass	2.60	0.06	±4.0%	-
		Fiberglass	4.46	0.36	±6.0%	
		Teflon	2.09	0.003	±6.0%	
	94	Plexiglass	2.54	0.08	±8.0%	
		Fiberglass	4.42	0.41	±9.0%	
		Teflon	2.07	0.006	±6.0%	
[31]	93.788	Teflon	2.065	0.002	±2.0%	±15%
		Rexolite	2.556	0.003	±2.0%	±24%
		TPX	2.150	0.0010	±2.0%	±10%
		Fused quartz	3.510	0.0010	±2.50%	±10%
		36D	2.485	0.0012	±2.0%	±19%
		36DA	3.980	0.0010	±2.0%	±7.5%
		36DK	5.685	0.0040	±2.0%	±2.5%
		36DS	1.765	0.0042	±2.5%	±2.5%
[34]	16.0	Fused quartz	3.85	-	±1.5%	-
		Teflon	2.02	-	±2.0%	-
		PVC	2.93	0.0046	±1.5%	±35%
[38]	77	Glass	6.782	0.0278	< ±1.0%	< ±2.0%
	94	Glass	6.765	0.0296	< ±1.0%	< ±2.0%
[41]	6.2	Polystyrene-Glass epoxy	2.88(3.06)	0.017(0.036)	-	-
[43]	30	PTFE glass fiber	2.29	-	-	-
		Polymer alloy	3.03	-	-	-
		Hydrocarbon ceramic	3.46	-	-	-
		TMM4 (Ceramic polymer)	4.77	-	-	-
		PTFE ceramic	6.41	-	-	-
		N-type 5000 ohm-cm silicon	11.20	-	-	-
[46]	72-110	PVC	2.931	0.01002	-	-
		Alumina ADS-96R	8.85	<0.001	-	-
		Rexolite 1422	2.534	0.0013	-	-
		Polyetherimide PEI	3.063	0.0074	-	-
		Polymer	2.665	0.0407	-	-
		Plywood	2.371	0.0578	-	-
[56]	110	Teflon	2.04	0.001	±4.0%	±100.0%
		PMMA	2.61	0.012	±4.0%	±100.0%
		PVC	2.88	0.011	±4.0%	±100.0%
[60]	750-1100	Silicon	11.19	-	-	-
		HR-Si	11.57	-	-	-
		HR-GaAs	13.01	-	-	-
		Polystyrene	2.45	-	-	-
[62]	26-40	Plexiglass	2.59	1.14e-2	2.9%	32%
		PVC	2.64	8.45e-3	1.9%	35%
		PETP	2.25	3.41e-3	3.2%	31%
		Mortar	6.93	6.74e-1	0.8%	43%
		Nylon	2.95	8.47e-2	1.3%	13%
		Polypropylene	2.24	2.56e-2	0.8%	28%
[64]	325-500	Teflon	2.02-2.04	-	0.5%	-
		PMMA	2.58-2.61	-	0.5%	-
		PVC	2.87-2.90	-	0.5%	-
[72]	110	Alumina	8.059	0.001	0.5%	-
		Zirconium oxide	23.52	0.001	0.5%	20%
		Boron nitride	4.178	0.004	0.5%	50%
		Silicon nitride	5.138	0.016	0.5%	9%

Talbe III Measurement uncertainty comparison between transmission line and resonator methods

Ref	Materials	Frequency (GHz)	Method	Accuracy
[94]	Liquid crystal polymer, Teflon	33-50	Transmission line (rectangular dielectric waveguide)	5% for ε_r', not mentioned for $\tan\delta$
[95]	Liquid crystal polymer, PTFE, Alumina, Methyl methacrylate	80-110	Transmission line (rectangular dielectric waveguide)	2.5%-4.0% for ε_r', not mentioned for $\tan\delta$
[96]	Silicon Oxide,	0-40	Transmission line	5% for ε_r', not mentioned for $\tan\delta$
[77]	PTFE	3	Transmission line	<2% for ε_r',<3% for $\tan\delta$
[80]	PTFE	8-13	Transmission line	<2% for ε_r'
[97]	Teflon, Polystyrene, plexiglass, Rexolite, Polyethylene	10, 25, 143, 343	Open resonator	<0.5% for ε_r', not mentioned for $\tan\delta$
[98]	fused Silica	94	Open resonator	<0.2% for ε_r', <10% for $\tan\delta$
[99]	Alumina, polypropylene	28-36	Open resonator	0.5% for n ($\sqrt{\varepsilon_r'}$)
[100]	Polyethylene, Polypropylene, Sapphire	60	Open resonator	0.1% for ε_r', 5% for $\tan\delta$
[101]	Yttrium Iron Garnet	60	Open resonator	<0.2% for ε_r', <10% for $\tan\delta$